# Observation of regional air pollutant transport between the megacity Beijing and the North China Plain

Yingruo Li[1], Chunxiang Ye[1,2], Jun Liu[1], Yi Zhu[1], Junxia Wang[1], Ziqiang Tan[1], Weili Lin[3], Limin Zeng[1], Tong Zhu[1,4*]

[1]State Key Laboratory of Environmental Simulation and Pollution Control, College of Environmental Sciences and Engineering, Peking University, Beijing, 100871, China

[2]Now at School of Chemistry, University of Leeds, Leeds LS2 9JT, UK

[3]Meteorological Observation Center, China Meteorological Administration, Beijing, 100081, China

[4]The Beijing Innovation Center for Engineering Science and Advanced Technology, Peking University, Beijing, 100871, China

*Corresponding Author: tzhu@pku.edu.cn

**Abstract.** Megacities have strong interactions with the surrounding regions through transport of air pollutants. It has been frequently addressed that the air quality of Beijing was influenced by the influx of air pollutants from the North China Plain (NCP). Estimations of air pollutant cross-boundary transport between Beijing and the NCP is important for air quality management. However, evaluation of cross-boundary transport using long-term observations is very limited. Using the observational results of the gaseous pollutants $SO_2$, NO, $NO_2$, $O_3$, and CO from August 2006 to October 2008 at the Yufa site, a cross-boundary site between the megacity Beijing and the NCP, together with meteorological parameters, we explored the transport directions and evaluated the transport flux intensity at Yufa, as part of the "Campaign of Air Quality Research in Beijing and Surrounding Region 2006–2008" (CAREBeijing 2006–2008). The hourly mean ± SD (median) concentration value of $SO_2$, NO, $NO_2$, $NO_x$, $O_3$, $O_x$, and CO were 15 ± 16 (9) ppb, 12 ± 25 (3) ppb, 24 ± 19 (20) ppb, 36 ± 39 (23) ppb, 28 ± 27 (21) ppb, 52 ± 24 (45) ppb, and 1.6 ± 1.4 (1.2) ppm during the observation period from 01 September 2006 to 31 August 2008, respectively. The bivariate polar plots showed the dependence of pollutant concentrations on both wind speed and wind direction, and thus inferred their dominant transport directions. Surface flux intensity calculations further demonstrated the regional transport influence of Beijing and the NCP on Yufa. The surface transport flux intensities (mean ± SD) of $SO_2$, NO, $NO_2$, $NO_x$, $O_3$, $O_x$, and CO were 6.2±89.5, -4.3±29.5, -0.6±72.3, -4.9±93, 14.7±187.8, 14.8±234.9, and 70±2830 μg $s^{-1}$ $m^{-2}$ during the observation period, respectively. For $SO_2$, CO, $O_3$, and $O_x$ the surface flux intensities from the NCP to Yufa surpassed those from Beijing to Yufa in

all seasons except winter, with the strongest net fluxes largely in summer, which is about 4–8 times of other seasons. The surface transport flux intensity of $NO_x$ from Beijing to Yufa was stronger than that from NCP to Yufa except in summer, with the strongest net flux in winter, which is about 1.3–8 times of other seasons. Considering limitation of the spatial representation of the Yufa site, the PSCF analysis based on the HYSPLIT-4 model was used to validate the results of the surface flux intensities calculation. Our study also suggested that various factors, such as the wind field, emission inventory, and photochemical reactions, could influence the transport of air pollutants. The decrease of surface flux intensity during the Olympic Games period implied that both local emission reduction and regional cooperation must be considered in air quality management. More multidimensional data are needed for further comprehensive discussion of the regional transport between Beijing and the NCP.

**Keywords:** Megacity Beijing, North China Plain, Yufa site, Regional transport, Long-term and multiple-species observation

## 1. Introduction

Megacities are large sources of air pollutants and greatly influence the surrounding areas (Parrish and Zhu, 2009). With a population over 20 million, the city of Beijing is an example of such a megacity. Beijing has faced severe air pollution problems over the past two decades and has intensive interactions with other emission hot spots within the North China Plain (NCP) (Chen et al., 2015; Shao et al., 2006; Zhang et al., 2012). Beijing and the NCP are surrounded by the Yanshan Mountains to the north

and the Taihang Mountains to the west. The semi-basin geographical features together with the continental monsoon climate make regional transport of air pollutants between the megacity Beijing and the NCP an important factor affecting air quality in Beijing and the NCP (An et al., 2007; Guo et al., 2010; Lin et al., 2008, 2009; Streets et al., 2007; Wang et al., 2006; Wang et al., 2011; Wang et al. 2015; Wu et al., 2011; Xu et al., 2005; Xu et al., 2011). An improved understanding of the regional transport of air pollutants between Beijing and the NCP is therefore essential for air quality management of the megacity Beijing and establishment of regional-scale emissions control measures.

Previous studies have shed light on the regional transport sources of the megacity Beijing, and various techniques have been employed, including rural/urban station observations (Guo et al., 2010; Lin et al., 2008, 2009; Wang et al., 2006; Xu et al., 2011), mobile laboratory measurements (Wang et al., 2009, 2011; Zhu et al., 2016), and modelling studies (An et al., 2007; Matsui et al., 2009; Wu et al., 2011). A ground-based observation study from July 2006 to September 2007 at the Gucheng site (Lin et al., 2009), a rural site south-west of Beijing, found that high concentrations of gaseous pollutants, including nitric oxide (NO), nitrogen dioxide ($NO_2$), nitrogen oxides ($NO_x$=NO+$NO_2$), sulphur dioxide ($SO_2$), carbon monoxide (CO), ozone ($O_3$), and Oxidant ($O_x$=$NO_2$+$O_3$), were accompanied by air masses moving northward from Gucheng to Beijing, according to back-trajectory analysis. Similar to Lin et al. (2009), regional transport of air pollutants between Beijing and the NCP was observed consistently in these previous studies (Lin et al., 2008; Yuan et al., 2009; Zhu et al., 2011), even though they were merely short-term observations.

Many studies have also attempted to quantify transport fluxes of the main gaseous pollutants. A mobile laboratory study in Beijing city demonstrated regional transport of $SO_2$ from the NCP in both emission-control and non-control scenarios during the Beijing 2008 Olympics (Wang et al., 2011). Extrapolated from five 1-day case studies, the annual transport fluxes of $SO_2$ through the south-east part of the 6th Ring Road into Beijing were estimated at 49.2 Gg $yr^{-1}$ and 146.3 Gg $yr^{-1}$, accounting for 70 % and 73 % of the annual $SO_2$ emissions in Beijing under emission-control and non-control scenarios, respectively. The Community Multi-scale Air Quality (CMAQ) model simulation by An et al. (2007) found that the regional transport from the surrounding areas of Beijing can contributed 39 % of $PM_{2.5}$, 30 % of $PM_{10}$, and 18 % of $SO_2$ to the city on average in a heavy pollution episode in the spring of 2005. Similarly, the CMAQ model simulation over the Beijing region for July 2001, reported by Streets et al. (2007), illustrated the regional transport of secondary $PM_{2.5}$ and $O_3$ between Beijing and the NCP. The study suggested that the average contributions of regional transport to $PM_{2.5}$ concentrations in the megacity Beijing from Hebei Province, Shandong Province, and Shanxi Province were about 32 %, 11 %, and 3.5 %, with maximum contributions of 70 %, 63 %, and 21 %, respectively. The regional transport contributions to the concentrations of $O_3$ in Beijing were less significant, with maximum contributions of 28 % from Hebei Province, 24 % from Shandong Province, and 10 % from Shanxi Province, respectively.

In summary, long-term observation of transport flux is necessary to constrain regional models and to directly evaluate the influence of regional transport on air quality. Estimations of air pollutant cross-boundary transport between Beijing and

NCP is important for air quality management. However, evaluation of cross-boundary transport using long-term observations is very limited. In this study, we developed a method of calculating the surface transport flux intensity across a cross-boundary site based on long-term ground-based measurement and evaluated the regional transport influence of Beijing and the NCP on the cross-boundary site. The results showed different transport directions and seasonal variations in the surface transport flux intensities of the main pollutants, including $SO_2$, NO, $NO_2$, $NO_x$, $O_3$, and CO at the Yufa site. The key factors controlling regional transport are also discussed, which is important for the establishment of air quality control policy in future.

## 2. Measurements and Methods

### 2.1. Measurements

The Yufa site is located at the cross-boundary area between Beijing and the NCP and could be influenced by emissions from the megacity Beijing and long-range transport from the NCP. The measurements at the Yufa site (39°30'49"N, 116°18'15"E) were conducted from the top of a building (about 20 m above ground level) on the campus of Huangpu College. There is no tall building around the Yufa site which affects the wind and gas measurements. This is a rural site about 50 km south of the center of Beijing and near the border of Beijing Municipality and Hebei Province. As shown in Fig. 1, the Yufa site locates in the temperate monsoon climate zone and the topography of the surrounding area is flat (Fig.1), the prevailing wind is the same as the surrounding region (Lin et al., 2009). Thus the wind field of the Yufa site is representative in the researched area in this study. The northern and western sides

of the site are mountain areas where the dry and clean air masses come from, whereas the southern and south-eastern sides are surrounded by heavily industrialised and urbanised areas, such as Hebei Province and Tianjin City (Fig.1).

Figure 1. here

The gaseous pollutant species measured included $SO_2$, NO, $NO_2$, $NO_x$, $O_3$, and CO. $SO_2$ was measured using a sulphur dioxide analyser (9850B; Ecotech, Knoxfield, Australia) which combines microprocessor control with pulsed UV fluorescence detection with the precision of 0.5 ppb and uncertainty within 10 %. The detection limit for the analyser is 0.5 ppb and the time resolution is 1 min. Reactive nitrogen species (NO, $NO_2$, and $NO_x$) were measured using nitrogen analyser (9841B; Ecotech) which utilises microprocessor control and chemiluminescence detection with the precision of 0.5 ppb and uncertainty within 10 %. The detection limit for the instrument is 0.5 ppb and the time resolution is 1 min. CO was measured using a CO analyser (9830A; Ecotech) which utilises NDIR Gas Filter Correlation photometry and microprocessor control with the precision of 0.1 ppm and uncertainty within 1 %. The detection limit for the instrument is 50 ppb and the time resolution is 1 min. $O_3$ was measured using an ozone analyser (9810B; Ecotech) which combines microprocessor control with UV photometry with the precision of 1 ppb and uncertainty within 5 %. The detection limit for the instrument is 0.4 ppb and the time resolution is 1 min. Measurements of meteorological parameters, including wind direction (WD), wind speed (WS), temperature (T), barometric pressure (BP), and relative humidity (RH), were conducted with a LASTEM auto meteorology station (LASTEM, Milan, Italy). All trace gas instruments were maintained and calibrated

routinely following the manufacturer's protocols. The main reasons for missing data were power and instrument failure. The detail information of the instruments was listed in Table 1.

Table 1. here

**2.2. Methods**

**2.2.1. Transport direction analysis**

The transport of gaseous pollutants is markedly influenced by meteorological parameters, especially wind speed and wind direction. For local emission sources, wind can facilitate the dilution and diffusion of air pollutants. Strong wind usually has marked diffusion capability, whereas weak wind usually leads to accumulation of air pollutants. For regional sources, strong wind can transport pollutants over long distances and may result in high concentrations of pollutants in downwind areas. Therefore, the relationship between pollutant concentration and wind field is an indicator of regional transport.

The bivariate polar plot graphical technique was used to investigate the relationships between the concentrations of gaseous pollutants and wind field, and to identify potential emissions sources and transport directions of air pollutants according to the technique developed by Carslaw et al. (2006) and Westmoreland et al. (2007). The variables (such as pollutant concentrations, wind speed, and wind direction) were plotted in polar coordinates. The procedure was as follows. First, the concentration data were partitioned into wind speed-wind direction bins, and the

mean concentrations were calculated within each bin. Then, the wind components *u* and *v* were calculated using Eq. (1):

$$u = \mathrm{WS} \cdot \sin(\pi\theta/180), v = \mathrm{WS} \cdot \cos(\pi\theta/180) \quad (1),$$

where WS is the hourly mean wind speed, and $\vartheta$ is the wind direction in degrees, with 90° being from the east. Then, a generalised additive model (GAM; Jayamurugan et al., 2013) was used for surface fitting to describe the concentration as a function of the wind components *u* and *v*. The concentrations calculated by the GAM can be expressed with Eq. (2):

$$\sqrt{C_i} = \beta_0 + s(u, v) + e_i \ (2),$$

where $C_i$ is the calculated pollutant concentration, $\beta_0$ is the overall mean of the response, $s(u,v)$ is the smooth function, and $e_i$ is the residual.

Compared to the nonparametric regression used by Henry et al. (2002), the bivariate polar plot involves the dependence of pollutant concentration on both wind speed and wind direction. The non-linear relationships among the variables (such as concentrations of gaseous pollutants, wind speed, and wind direction) as well as the interactions among these variables can be considered using the GAM method for data smoothing. In addition, the use of polar coordinates makes the graphics more intuitive.

**2.2.2. Transport flux assessment**

The surface transport fluxes at the Yufa site were calculated with the following formula (White et al., 1976; Wang et al., 2011):

$$f = -\frac{1}{n}\sum_{j=1}^{n} C_j \times WS_j \times cos\theta_j \quad (3),$$

$$\sigma = H_0 \times L_0 \quad (4),$$

$$FLUX = f \times \sigma \quad (5),$$

where $f$ is surface flux intensity of the pollutants, i.e. the per unit area flux (μg $s^{-1}$ $m^{-2}$); $C_j$ is the mean concentration of the pollutants (μg $m^{-3}$) during the $j$th observation hour; $\vartheta_j$ is the angle between the wind direction and the north-south direction during the $j$th observation hour; and $WS_j$ is wind speed (m $s^{-1}$) during the $j$th observation hour; n is the total number of observation hour; $\sigma$ is the surface cross-sectional area ($m^2$) with the width of $L_0$ (m) and height of $H_0$ (m); the average surface flux of the pollutants (i.e. FLUX) (μg $s^{-1}$) can be obtained by multiplying flux intensity f and the cross-section area $\sigma$.

Figure S1 shows a schematic diagram of the surface flux calculation. The flux intensity here is the product of wind sector and air pollutant concentration measured at the same location. Ideally, we need to use the wind speed and air pollutant concentration with infinite small time resolution to conduct the surface flux calculations. In this study, the hourly data of the pollutants and wind were used, mainly because the pollutants concentration data was converted from the minutes' data to hourly mean to remove the accidental fluctuation and reduce the noise. Therefore, we assumed the wind speed and wind direction were constant within one hour, and hourly wind data were used to match with the hourly air pollutant concentration data to calculate the flux intensity.

It also need to make it clear that the surface flux intensity calculated in this study is the per unit area flux across the Yufa site, which is different from the flux across a large area reported in other studies (e.g. Wang et al. 2011). Our results could only be

extrapolated if the concentrations of all the pollutants, wind speed and direction were homogenously distributed, vertically and horizontally. Otherwise, vertical profiles of air pollutants concentration and wind are needed to calculate the cross-section transport flux of two adjacent regions for the whole boundary layer with the integrating formula below:

$$FLUX = \iint C_{(x,z)} WS_{(x,z)} sin\theta_{(x,z)} dxdz = \iint f_{(x,z)} dxdz \quad (6),$$

where x is horizontal distance to the observed point, z is the vertical distance from ground to the observed point. In this study, we only focus on the method developing of the surface flux intensity calculation and evaluation of the regional transport influence of Beijing and the NCP on the cross-boundary site based on the ground-based observation data.

**2.2.3 The backward trajectory model and PSCF analysis**

The 12 h air mass back trajectories arriving at the Yufa site at 500 m above the ground level were calculated using the National Oceanic and Atmospheric Administration (NOAA) Hybrid Single-Particle Lagrangian Integrated Trajectory Version 4 model (HYSPLIT-4 model) (http://ready.arl.noaa.gov/HYSPLIT.php) during the study period (from 15 August 2006 to 31 October 2008) with a 1˚ × 1˚ latitude–longitude horizontal resolution and the final meteorological database. The final archived meteorological data was obtained from the National Center for Environmental Prediction's (NCEP's) Global Data Assimilation System (GDAS) (ftp://arlftp.arlhq.noaa.gov/pub/archives/gdas1). The back trajectories were

generated with 6-h time resolution (four times per day) at starting times of 0:00, 6:00, 12:00 and 18:00 UTC (8:00, 14:00, 20:00, 4:00 LT-local time, respectively).

The potential source contribution function (PSCF) analysis were performed with the Gis-based software TrajStat (http://www.meteothinker.com/products/trajstat.html) (Wang and Zhang et al., 2009). The PSCF analysis has been widely used for identifying the possible source areas of the observed high concentrations of pollutants at the receptor site (Ashbaugh et al., 1985; Zhang et al., 2013). The study domain was divided into i × j equal grid cells and the PSCF value for *ij*th cell is defined as:

$$\mathrm{PSCF}_{ij} = m_{ij} / n_{ij} \quad (7),$$

where $n_{ij}$ denoted the number of endpoints that fall in the *ij*th cell, and $m_{ij}$ represented the number of endpoints for the same cell having arrival times at the observed site corresponding to measured data higher than an arbitrarily set criterion.

To reduce the effect of small values of $n_{ij}$, the PSCF values were multiplied by an arbitrary weigh function $W_{ij}$. In this study, $W_{ij}$ is defined as below.

$$W_{ij} = \begin{cases} 1.00, & 80 < n_{ij} \\ 0.70, & 20 < n_{ij} \leq 80 \\ 0.42, & 10 < n_{ij} \leq 20 \\ 0.05, & n_{ij} \leq 10 \end{cases} \quad (8),$$

In this study the long-term calculated surface flux intensity data was assigned to the corresponding trajectories in the PSCF analysis to investigate whether the transport surface flux intensity calculation at the Yufa site be consistent with the air mass movement direction from Beijing and NCP to the Yufa site. The study domain was 30–50 ˚ N, 100–130 ˚ E and the horizontal resolution was 0.25 ˚ × 0.25 ˚.

## 3. Results and discussion

### 3.1. Observations

Figure 2. here

The time series of hourly average and 24-hour smoothing concentrations of $SO_2$, NO, $NO_2$, $NO_x$, $O_3$, $O_x$, and CO observed at the Yufa site from 15 August 2006 to 31 October 2008 are shown in Fig. 2. The hourly mean±SD (median) concentration value of $SO_2$, NO, $NO_2$, $NO_x$, $O_3$, $O_x$, and CO were 15 ± 16 (9) ppb, 12 ± 25 (3) ppb, 24 ± 19 (20) ppb, 36 ± 39 (23) ppb, 28 ± 27 (21) ppb, 52 ± 24 (45) ppb, and 1.6 ± 1.4 (1.2) ppm during the observation period from 01 September 2006 to 31 August 2008, respectively, with hourly mean values -3, 1, 6, 7, -1, 5 and 0 ppb higher for $SO_2$, NO, $NO_2$, $NO_x$, $O_3$, $O_x$, and CO than the Gucheng site, a polluted rural site to the south-west of Beijing, from July 2006 to September 2007 (Lin et al., 2009). The hourly mean values were 12, 11, 17, 28, -5, 22 and 972 ppb higher than those observed at the clean background at the Shangdianzi site, which is one of the regional Global Atmosphere Watch (GAW) stations in China over the period 2004–2006 (Lin et al., 2008). The compared results indicating that Yufa site has become a relatively polluted rural site. Typical seasonal variations were observed for all gaseous pollutants. Concentrations of primary pollutants, including $SO_2$, NO, $NO_2$, $NO_x$, and CO, were high in winter and low in summer. In contrast, those of secondary pollutants, such as $O_3$, were high in summer and low in winter.

Figure 3. here

284 Meteorological parameters such as WS, WD, RH, T, and BP were also measured
285 at the Yufa site; the monthly statistics are shown in Fig. 3. North (usually in winter) or
286 south wind (usually in summer) prevailed at the Yufa site, with monthly average wind
287 speed mostly below 2 m $s^{-1}$. Exceptional conditions occurred occasionally in spring
288 and winter for the north wind, with monthly average wind speeds around 2–3 m $s^{-1}$.
289 In addition, for the north wind, the mean speed was higher than the median speed,
290 suggesting the prevalence of high wind speeds in both spring and winter. Prevailing
291 north wind with high wind speed during winter and spring has been reported
292 consistently in the Beijing area (Lin et al., 2008; Wehner et al., 2008). Another
293 exceptional condition occurred in spring for the south wind, with a monthly average
294 wind speed around 2 m $s^{-1}$. Figure 4 summarises the prevalence of wind direction in
295 the four seasons. Generally, the prevailing surface wind directions were north-
296 northeast and south-southwest in all seasons. In winter and spring, winds from the
297 north-northeast sector made a contribution of about 40–50 % to wind frequency.
298 Whereas under the influence of summer monsoon, winds from south increased
299 significantly in summer, with the contribution to wind frequency above 40 %. RH was
300 higher in summer and lower in spring and winter with the driest month in April of
301 2007 and February of 2008. The seasonal variation of RH may partially be related to
302 the variations of WS (Lin et al., 2011). T was higher in summer and lower in winter.
303 Surface pressure measurements showed high values in winter and low values in
304 summer due to surface heating and lifting air masses in summer, which partly
305 accounted for the wind field in the NCP (Takegawa et al., 2009).

306 Figure 4. here

The seasonal variations in gaseous pollutants and meteorological parameters could be linked in certain ways. For example, the high temperature and low pressure in summer suggested a high boundary layer and diluted gaseous pollutants to some extent. The high temperature, light intensity, and relative humidity also favoured the chemical transformation of these primary pollutants and the formation of secondary pollutants. The high wind speeds in spring and winter also affected regional transport, and therefore the concentrations of gaseous pollutants, as discussed below.

### 3.2. Transport direction

#### 3.2.1. The bivariate polar plots for the whole observed period

As shown in Fig. 1, the Yufa site located at the boundary area of Beijing city and the NCP. Prevalent south/south-west or north/north-east wind would bring in polluted or clean air masses to the site. Air masses from both directions would pass over the Yufa site. Regional transport from the megacity Beijing and the NCP could therefore be observed at the Yufa site. The transport directions for gaseous pollutants, including $SO_2$, NO, $NO_2$, $NO_x$, $O_3$, $O_x$, and CO, will be discussed in this section.

Figure 5. here

Figure 5a-g show the bivariate polar plots for $SO_2$, NO, $NO_2$, $NO_x$, $O_3$, $O_x$, and CO at the Yufa site, respectively. In the low wind speed scenario, high or medium concentrations of NO, $NO_2$, $NO_x$, $SO_2$, and CO were generally observed, along with low $O_3$ and $O_x$ concentrations. In the high wind speed scenario, the dependence of species concentration on wind speed and wind direction was more varied.

329 Specifically, the bivariate polar plot in Fig. 5b clearly shows dependence of high NO
330 concentration (higher than 30 ppb) on low wind speed, with low NO concentration
331 (lower than 5 ppb) at wind speeds > 3 m $s^{-1}$. The bivariate polar plot in Fig. 5c shows
332 similar dependence of high $NO_2$ concentration on low wind speed, but $NO_2$
333 concentrations up to 20 ppb were still observed with medium wind speeds of around
334 5 m $s^{-1}$ from the south, east, and north-east. Accordingly, the dependence pattern of
335 the $NO_x$ concentration (Fig. 5d) on wind speed and wind direction reflected the
336 features of both NO and $NO_2$. The dependence pattern of high CO concentration on
337 low wind speed in Fig. 5g was similar to that for $NO_x$, but a considerable CO
338 concentration, substantially higher than background level, was still observed at wind
339 speeds exceeding 5 m $s^{-1}$ from the south and the east. Figure 5a shows similar
340 dependence of medium-high concentration of $SO_2$ (around 20 ppb) on low wind
341 speed, with one unique feature being that high $SO_2$ concentration was observed
342 under conditions of high wind speed (> 5m $s^{-1}$) in various wind directions (especially
343 the south wind). Finally, the bivariate polar plot in Fig. 5e shows the dependence of
344 $O_3$ concentration on wind speed and wind direction, which was somewhat opposite
345 to the patterns for other species. The low $O_3$ concentration (< 20 ppb) was related to
346 low wind speed or calm wind conditions. With the north wind and medium or high
347 wind speed, a typical background $O_3$ concentration (around 50 ppb) was observed.
348 With south wind and medium or high wind speed, high $O_3$ concentration was
349 observed. The dependence of the high $O_x$ concentration on high wind speed from the
350 south and south-east was similar to that of $O_3$, but no low concentration of $O_x$ was

observed under low wind speed conditions (Fig. 5f)., probably due to the compensation of high $NO_x$ concentration at low wind speeds (Fig. 5d).

Figure 6. here

The high concentrations of NO, $NO_2$, $NO_x$, and CO and the medium-high concentration of $SO_2$ observed under low wind speed conditions were consistent with their high emission intensities in the Beijing area (Fig. 6). Due to the marked increase in the number of vehicles and heavy energy consumption, Beijing has been a well-known emission hot spot for NO and $NO_2$ (Tang, 2004). Meanwhile, the extremely high levels of CO emissions in the Beijing area are clearly shown in the emissions map (Fig. 6) and have been reported consistently (Wang et al., 2009) and directly observed, with peak CO concentrations up to 9.3 ppm. Only medium-high $SO_2$ concentration (~15 ppb) observed even at low wind speed suggested the successful reduction of $SO_2$ emission, which could be ascribed to the continuous effort of the Chinese government since the 1990s and during the Olympic Games (Tang, 2004; Wang et al., 2009, 2011; Qin et al., 2009). Accordingly, the $O_3$ concentration under low wind speed conditions was lower than the typical background level, which could be attributed to the rapid titration of $O_3$ by of accumulation NO.

### 3.2.2 Seasonal variations of the bivariate polar plots

Figure 7. here

The different patterns of the bivariate polar plots reflected the differences in local emission and regional transport for different species. The emissions, the

meteorological conditions, the chemical reaction rate and the species lifetime, which have essential influence on the regional transport, varied greatly by seasons. Thus the seasonal variations of the bivariate polar plots and the corresponding causes of the variations were discussed in this section.

Figure 7b-d show seasonal variations of the bivariate polar plots for NO, $NO_2$, and $NO_x$ at the Yufa site, respectively. Generally, the mean concentrations of $NO_2$, $NO_x$ and especially NO in the low wind speed scenario are higher than those in the higher wind speed scenario in all the seasons. The mean concentration of NO is less than 10 ppb when the wind speed higher than 5 m $s^{-1}$ in all seasons (Fig. 7b). Figure 7c clearly shows the relatively higher concentration of $NO_2$ (~20 ppb) with winds at the wind speed >5 m $s^{-1}$ from the south sector in spring, from the northeast and south sectors in summer and winter, and from the northeast sector in autumn. Figure 5d shows the dependence pattern of $NO_x$ is similar to both NO and $NO_2$. Although emission hot spots of NO, $NO_2$, and $NO_x$ are widespread in the NCP, the long-range transport of these species to Yufa is limited by the lifetime of these species. As the average $O_3$ concentrations is for spring, summer, autumn and winter is 20, 11, 32, and 42 ppb respectively at the Yufa site, the corresponding typical lifetime of NO is 51 s in summer, 66 s in spring, 106 s in autumn, and 181 s in winter, respectively, just assuming all the NO is removed mainly by chemical reaction with $O_3$ (Sander et al., 2011). The transport distance of NO is therefore less than 5 km even with a high wind speed of 15 m $s^{-1}$. Even when considering the the conversion of NO from $NO_2$ with conversion efficiency ~30 % in summer and autumn (Takegawa et al. 2009), the transport distance of NO is still limited, for the lifetime of $NO_2$ is also

relative short (Beirle et al., 2011; Gu et al., 2013). That is, NO concentration is determined by local emissions rather than regional transport. $NO_2$ and $NO_x$ have slightly longer lifetimes in the atmosphere than NO has, typically on the order of 4-5 h and with slightly shorter photochemical lifetime in warm seasons (Beirle et al., 2011; Gu et al., 2013). Hence, the typical transport distance of these species is around 100 km at the wind speed of 5 m $s^{-1}$ (Beirle et al., 2011). Within such transport distance, the Yufa site is surrounded by various $NO_x$ emission hot spots (Fig. 6), such as the megacity Beijing to the north, the Baoding-Cangzhou area to the south, and the Tianjin-Tangshan area to the east. Meanwhile the emission intensity is larger in winter and autumn than that in spring and summer (Fig. 6). It is therefore reasonable to observe the influence of short-range transport, in addition to local emissions, on the local $NO_2$ and $NO_x$ concentrations, especially in the cold seasons (Fig. 7c and 7d). Although our results suggested that short-range transport from these surrounding areas, especially the urban area of Beijing, was a non-negligible factor affecting the local $NO_x$ concentration at the Yufa site, the regional transport of $NO_x$ is of less significance compared to $SO_2$ and CO due to its limited transport distance (see below).

Figure 7e is the seasonal bivariate polar plots of CO, which clearly shows the relatively higher mean concentration of CO (> 1 ppm) with winds at low wind speed (< 2 m $s^{-1}$), which similar to nitrogen oxide species. The mean concentration of CO was relatively higher with wind at higher wind speed (> 5 m $s^{-1}$) also from south sector in spring and summer, from northeast and south sector in autumn, and from north and south in winter. The oxidation lifetime of CO is typically ~20 days, under

419 the assumption of OH radical concentration of $2 \times 10^6$ $cm^{-3}$ (Xu et al., 2011). This is
420 substantially longer than the lifetime of $NO_x$, making regional transport of CO an
421 important process affecting local air quality in the downwind area. The different
422 lifetimes of CO and $NO_x$ appeared to explain the unique high concentration of CO,
423 but not $NO_x$, at wind speeds exceeding 5 m $s^{-1}$ from the south and the east. Our
424 results suggest that regional transport from the south and central NCP and the
425 Tianjin area could greatly affect local concentrations of CO at the Yufa site.

426 Figure 7a clearly shows the relatively higher mean concentration of $SO_2$ (20 ppb)
427 with winds at higher wind speed (> 5 m $s^{-1}$) from the south sector in spring and
428 summer. The mean concentration of $SO_2$ was relatively higher with wind at higher
429 wind speed (> 5 m $s^{-1}$) from the north-east, east, and south sectors in autumn and
430 winter. Similar to CO, $SO_2$ has a relatively long lifetime in the atmosphere compared
431 to $NO_x$, i.e. a couple of hours to 1–2 days with longer lifetime in winter and shorter
432 lifetime in summer (Beirle et al., 2014; He et al., 2012; Lee et.al., 2014), and regional
433 transport of $SO_2$ was expected to occur. Accordingly, regional transport from
434 emission hot spots located south of the Yufa site (Fig. 6), was found to influence the
435 local concentrations of $SO_2$ (Fig. 7a) in all seasons. Specifically, the highlighted
436 emission hot spots in the central NCP and the south NCP, which accounted for about
437 70 % of China's coal consumption in 10 % of China's domestic area (China Statistical
438 Yearbook, 2008), is a major source of $SO_2$ in the Beijing area by regional transport.
439 Furthermore, regional transport from north-east sector of the Yufa site, where the
440 center of the megacity Beijing located, also was observed in autumn and winter,
441 which indicated the increased emission of $SO_2$ in heating seasons.

Finally, the bivariate polar plot in Fig. 7f and 7g show the dependence of $O_3$ and $O_x$ concentration on wind speed and wind direction by season. The low $O_3$ concentration (< 20 ppb) was observed at low wind speed (< 2 m $s^{-1}$). With the north wind and wind speed > 5 m $s^{-1}$, a typical background $O_3$ concentration (around 50 ppb) was observed in spring and summer. With south wind and wind speed > 5 m $s^{-1}$, high $O_3$ concentration (above 60 ppb) was observed, especially in summer. The main difference of seasonal bivariate polar plots between $O_3$ and $O_x$ was that no low concentration of $O_x$ was observed under low wind speed conditions in all seasons. The low concentration of $O_3$ at low wind speed may be due to the titration of $O_3$ by NO, which more obvious in autumn and winter. Background $O_3$ levels in the north-west wind under medium and high speed conditions clearly reflect the transport of background air mass to the Yufa site from locations where the emission intensities of pollutants were relatively low (Fig. 6), and this is more obvious in spring when the air masses from the north-west increased (Fig. 4). Whereas $O_3$ concentrations higher than background level in the south wind under medium and high speed conditions especially in summer suggest accumulation of $O_3$ during its transport from the central NCP area or even the south NCP area to the Yufa site. Emission intensities of $O_3$ precursors, such as $NO_x$ and VOCs is high in the NCP, and the solar radiation is strong in summer, which facilitate the formation and transport of $O_3$ from NCP to Beijing (Zhang et al., 2014).

In conclusion, the emissions in the Beijing area are closely related to the observed concentrations of NO, $NO_2$, $NO_x$, and CO at Yufa. Regional transport had a clear influence on the concentrations of all gaseous pollutants examined here, with

the exception of NO. The emission hot spots located east, north-east, and especially south of the Yufa site determined the regional transport directions. The influence of regional transport differed among species. Regional transport of $SO_2$, CO, and $O_3$ from the central and south NCP to the Yufa site was more important, whereas regional transport of $NO_x$ from the NCP was less evident. Factors affecting regional transport included, but were not limited to, the atmospheric lifetime of pollutants, wind field, and local and regional emissions. As the Yufa site is a cross-boundary rural site between the megacity Beijing and the NCP, observation of transport flux there is appropriate in evaluating the regional transport influence by both the megacity Beijing and the NCP on the Yufa site.

### 3.3. Transport flux

#### 3.3.1 Seasonal variations of surface flux intensities

To evaluate the surface transport of the main air pollutants from Beijing and the NCP to the Yufa site, the surface flux intensities were calculated with Eqs. (3)-(5) based on observations at the Yufa site. The mean surface flux intensities in each season were also calculated for the 2-year observation period (Table 2). The overall net surface flux intensities (mean±SD) of $SO_2$, NO, $NO_2$, $NO_x$, $O_3$, $O_x$, and CO were 6.2±89.5, -4.3±29.5, -0.6±72.3, -4.9±93, 14.7±187.8, 14.8±234.9, and 70±2830 μg $s^{-1}$ $m^{-2}$ during the observation period from 01 September 2007 to 31 August 2008. The large standard deviation of the surface flux intensity indicated the large variations of the transport flux. Table 3 shows the mean IN (from the NCP to Yufa) surface flux intensities were highest in winter and lowest in summer, with the flux intensity value in winter 2–6 times of that in summer. The OUT (from Beijing to

Yufa) surface flux intensities show the same pattern, with the absolute flux intensity value in winter 2–8 times of that in summer. Yet the overall net transport surface flux intensities show quite different seasonal variations (Table 2) compared with the results in Table 3. For $SO_2$, CO, $O_3$, and $O_x$ the surface transport flux intensity from the NCP to Yufa surpassed those from Beijing to Yufa in all seasons except winter, with the strongest net fluxes largely in summer, which is about 4–8 times of other seasons. The net surface transport flux intensity of $NO_x$ from Beijing to Yufa was stronger than that from NCP to Yufa except in summer, with the strongest net flux in winter, which is about 1.3–8 times of other seasons.

Table 2. here

Table 3. here

To understand the transport fluxes reported here, it is necessary to discuss the affecting factors. First, the prevalent wind is a dominant factor affecting the surface fluxes. Figure 8 shows the time series of daily average surface flux intensity, i.e. the per unit cell flux (μg $s^{-1}$ $m^{-2}$) of $SO_2$, NO, $NO_2$, $NO_x$, $O_3$, $O_x$, and CO, and corresponding wind vectors (m $s^{-1}$) during the observation period. In general, the variations in the pollutant flux intensities showed a saw-teethed pattern, with positive (from the NCP to Yufa) and negative (from Beijing to Yufa) fluxes prevailing according to the shift in wind direction. Meanwhile, mainly due to the seasonal variations in wind speed and wind direction (Fig. 3 and 4), the magnitude of surface fluxes showed similar seasonal variation (Table 2). High net positive fluxes were observed in summer, and high net negative fluxes in winter. As the north wind

prevailed significantly over the south wind in winter, and the south wind over the north wind in summer (Fig. 4), the values of net surface flux intensities in these two seasons were the highest. During the other two seasons, frequent changes in positive and negative fluxes tended to cancel each other out, making the net transport fluxes less significant. This dominant role of wind field could also be illustrated by conditions during the winter of 2006/07. Exceptionally, the south wind prevailed in the winter of 2006/07 (Fig. 4), leading to the surface flux intensity of pollutants more positive in the winter of 2006/07 than 2007/08 (Table 2). For example, the increase of absolute surface fluxes strength for $NO_x$ between winter of 2006/07 and 2007/08 is on the order of a factor of 5.

Figure 8. here

Second, the transport flux is determined not only by the wind field but also by the emissions of pollutants in the upwind area. Various pollutants showed different patterns of seasonal variations in flux as a result of relative emission strengths in the upwind area compared to local emissions (Fig. 6). For example, the seasonal surface flux intensities of $SO_2$ were mainly positive, except in winter of 2007/08. The significant regional transport of $SO_2$ from the NCP to Yufa in all seasons except winter could be partly attributed to the high emission intensity of $SO_2$ in the NCP (Fig.6) and the reduction of $SO_2$ emission in Beijing (Wang et al., 2009, 2011; Qin et al., 2009), whereas the $SO_2$ flux output from Beijing was determined by the prevalent north wind, as explained above. In contrast to the net positive input flux of $SO_2$, the net seasonal surface flux intensities of CO were negative in both winter and autumn. The small output flux of CO in autumn reflected increased CO

emission in Beijing, which was sufficiently strong to account for the strong CO emissions in the NCP.

The influence of emissions on transport flux could also be inferred from an emissions-reduction scenario. For example, the 29$^{th}$ Olympic Games was held in Beijing during the period from 8 August 2008 to 20 September 2008. The Beijing government implemented aggressive long- and short-term air quality control measures in Beijing and its surrounding areas before and during the Olympic period to maintain good air quality during the Olympic Games (Wang et al.,2011; Wang et al., 2010). The control measures included moving the heavy polluted factories out the Beijing city, reducing the traffic emission through an odd/even plate number rule, and freezing construction activities (Wang et al., 2009). The concentrations of pollutants and the surface flux intensities during the 2008 Olympic Games were substantially reduced compared to the corresponding period of 2007 (Table 4). Besides the favored meteorological conditions (Fig. S2), the significant emission reduction both in the Beijing area and the NCP during the 2008 Beijing Olympic Games played a key role in the decrease of the transport flux intensities (Zhou et al., 2010).

Table 4. here

Finally, the chemical properties of these species could also affect the flux. Take $O_3$ for example, although both Beijing and the NCP are regarded as emissions hot spots for $O_3$ precursors, the short distance between Beijing and the Yufa site may hinder the secondary formation of $O_3$ to some extent. Thus the net surface transport of $O_3$ is from Yufa to Beijing, especially in summer time with an average

surface flux value of about 60 μg $s^{-1}$ $m^{-2}$. The lifetime of the pollutants also determined the different net transport flux intensities for different species (Table 2 and 3). The results are consistent with the results of bivariate polar plots we mentioned above (Fig. 7).

Overall, the flux intensities are influenced by at least the wind field, emissions inventory in both the upwind and local areas, and the chemical fates of these pollutants in the atmosphere. These observations provide insight for the analysis of projected transport flux under various emissions-reduction scenarios in the future. On the other hand, the dependence of the fluxes on these factors, which can vary, suggests that the fluxes reported here should not be compared with other reports under different conditions.

### 3.3.2 The back trajectory and PSCF analysis

The discussion above suggested the regional transport from both Beijing the NCP have important influence on the air quality of the Yufa site. However, both the bivariate polar plots and surface flux intensity calculation are based on the observation data at a ground measurement site. Considering the limitation of spatial representation of the Yufa site, the PSCF analysis based on the HYSPLIT-4 model was used to demonstrate the regional transport influence of the megacity Beijing and the NCP on Yufa in this section.

Figure 9. here

Figure 10. here

PSCF analysis was used in this study by combining backward trajectories and the corresponding surface transport flux intensities of pollutants. PSCF results of $SO_2$, NO, $NO_2$, $NO_x$, CO, $O_3$ and $O_x$ in 6-h resolution are shown in Fig. 9 for positive flux intensities (i.e from south to north) and in Fig. 10 for negative flux intensities (i.e. from north to south). It can be seen from Fig. 9, the higher PSCF values for most pollutants were located at the south-west area of the Yufa site, which indicate the positive surface flux intensities of the Yufa site is consistent with the air masses movement from south to Yufa. Figure 10 shows the higher PSCF values for most pollutants were located at the north area of the Yufa site, which indicate the negative surface flux intensities of the Yufa site is consistent with the air masses movement from north to Yufa. The PSCF analysis results validate the calculated flux intensities based on observation data can be used to evaluate the regional transport influence of Beijing and the NCP on the Yufa site. However, it should be noting that the PSCF results of NO, $NO_2$ and $NO_x$ was inconsistent with the flux calculation results sometimes (Fig. 9 and 10), which may partially ascribe to the uncertainty of flux calculation or the backward trajectories calculation. As a cross-boundary site between the megacity Beijing and the NCP, the surface flux intensities at the Yufa site may also indicate the transport between the megacity Beijing and the NCP.

### 3.3.3 Uncertainty and limitation

Uncertainty in calculation of the surface flux intensities in this study mainly come from the measurement of the pollutants and the wind. The uncertainty of the measurement for $SO_2$, $NO_x$, CO, and $O_3$ is within 10 %, 10 %, 1 %, and 5 %,

600 respectively. The uncertainty of wind speed is less than 5 % and the uncertainty of
601 wind direction is about 1 %. Thus the overall surface flux intensity calculation
602 uncertainty for $SO_2$, $NO_x$, CO, and $O_3$ is less than 12 %, 12 %, 6 % and 8 %.

603 In this study, we did not intent to extrapolate from Yufa site to the entire region.
604 We only focus on the method developing and evaluation of the regional transport
605 influence of Beijing and the NCP on the cross-boundary site based on the ground-
606 based observation data. Bivariate Polar plots analysis and surface flux intensity
607 calculation were conducted and get evidence of surface pollutants transport from
608 Beijing to the Yufa site and from the NCP to the Yufa site. Considering the variations
609 of the vertical and horizontal distributions of the air pollutants and meteorological
610 parameters, and influence of the boundary layer on the regional transport, more
611 multidimensional data with high precision and resolution are needed for further
612 comprehensive discussion of the regional transport between Beijing and the NCP.

613 **4. Conclusions**

614 We used 2-year observation data at a cross-boundary rural site between the
615 megacity Beijing and the NCP to investigate regional transport influence on the Yufa
616 site as part of the "Campaign of Air Quality Research in Beijing and Surrounding
617 Region 2006–2008" (CAREBeijing 2006–2008). The gaseous pollutants $SO_2$, NO, $NO_2$,
618 $NO_x$, CO, $O_3$, and $O_x$, together with meteorological data, were determined at Yufa
619 from August 2006 to October 2008. During the observation period, the average
620 concentrations of the pollutants at the Yufa site were relatively high, suggesting a
621 profound influence of the emissions from the megacity Beijing and regional transport
622 from the NCP.

Through bivariate polar plots, we found that the south wind, at relatively high wind speed, was essential for the inflow of $SO_2$, CO, and $O_3$ to from NCP to Yufa. For NO, $NO_2$, $NO_x$ and even CO, the emission from Beijing also played a dominant role. The seasonal variations of emission intensity, meteorological conditions, pollutant lifetimes make the regional transport of pollutants varied seasonally thus showed different bivariate polar plot patterns.

The seasonal variations in the surface flux intensities showed the strong net surface transport in summer from the NCP to Yufa and with net surface transport in winter for from Beijing to Yufa, mainly varying with the prevailing wind. The positive net fluxes of $SO_2$ and CO in this study infer a regional transport source of $SO_2$ and CO from the NCP to Yufa. Both positive and negative fluxes of $O_3$ could imply oxidant import from either the background areas to the north of Beijing or the NCP to the Yufa site, due to the titration effect of NO and further low $O_3$ level in Beijing. Whereas the fluxes of $NO_x$ here only indicated the influence of $NO_x$ emission in Beijing city could influence downwind area adjacent to Beijing, due to the limited transport distance of $NO_x$.

PSCF analysis demonstrated the regional transport from Beijing and NCP to Yufa can be evaluated by the surface flux intensity calculation based on the ground-based measurement data. As a cross-boundary site between the megacity Beijing and the NCP, the surface transport flux intensities at the Yufa site may also indicate the transport between the megacity Beijing and the NCP.

Our results again suggested that Beijing and the NCP have tight interactions through regional transport of air pollutants. Factors affecting the transport flux such

as meteorological parameters, especially wind speed and wind direction, emissions inventory, and photochemical reactions are essential for the regional transport fluxes and thus the air quality of the megacity Beijing and its surrounding areas. Therefore, both local emissions reduction and regional cooperative control should be taken considered in air quality management of Beijing.

**Author contribution**. T. Zhu designed the experiments and L. Zeng and the staff of the Yufa site carried out the experiment. Y. Li conducted the data analysis with contributions from all co-authors. J. Liu provided the emission maps. J. Wang managed the observation data of the program. Y. Li prepared the manuscript with the help of T. Zhu, C. Ye, J. Liu and Y. Zhu.

**Data availability.** The observation data of the Yufa site used in this paper is available on requests.

**Acknowledgements.** The authors express their sincere thanks to the staff of the Yufa site for carrying out the measurements. This work as part of CAREBeijing (Campaign of Atmospheric Researches in Beijing and surrounding area) was supported by Beijing Council of Science and Technology. This study was also supported by the National Natural Science Foundation Committee of China (21190051, 41121004, 41421064), the European 7th Framework Programme Project PURGE (265325), the Collaborative Innovation Center for Regional Environmental Quality.

The English in this document has been checked by at least two professional editors, both native speakers of English. For a certificate, please see:

http://www.textcheck.com/certificate/KcBduS

**References**


An, X., Zhu, T., Wang, Z., Li, C., and Wang, Y.: A modeling analysis of a heavy air pollution episode occurred in Beijing, Atmos. Chem. Phys., 7, 3103-3114, doi: 10.5 194/acp-7-3103-2007, 2007.

Ashbaugh, L.L., Malm, W.C., Sadeh, W.Z.: A residence time probability analysis of sulfur concentrations at Grand Canyon National Park. Atmos. Environ., 19 (8), 1263–1270,1985.

Beirle, S., Boersma, K. F., Platt, U., Lawrence, M. G., and Wagner, T.: Megacity emissions and lifetimes of nitrogen oxides probed from space, Science, 333, 1737-1739, doi:10.1126/science.1207824, 2011.

Beirle, S., Hörmann, C., Penning de Vries, M., Dörner, S., Kern, C., and Wagner, T.: Estimating the volcanic emission rate and atmospheric lifetime of $SO_2$ from space: a case study for Kīlauea volcano, Hawai`i, Atmos. Chem. Phys., 14, 8309-8322, doi:10.5194/acp-14-8309-2014, 2014.

Carslaw, D. C., Beevers, S. D., Ropkins, K., and Bell, M. C.: Detecting and quantifying aircraft and other on-airport contributions to ambient nitrogen oxides in the vicinity of a large international airport, Atmos. Environ., 40, 5424-5434, 2006.

Chen, H. S., Li, J., Ge, B. Z., Yang, W. Y., Wang, Z. F., Huang, S., Wang, Y. L., Yan, P. Z., Li, J. J., Zhu, L. L., Modeling study of source contributions and emergency control effects during a severe haze episode over the Beijing-Tianjin-Hebei area. SCIENCE CHINA Chemistry, 58 (9): 1403-1415, 2015.

China Statistical Yearbook 2008 (Beijing: China Statistic Press) (in Chinese).

693 Gu, D., Wang, Y., Smeltzer, C., and Liu, Z.: Reduction in NOx Emission Trends over
694 China: Regional and Seasonal Variations, Environ. Sci. Technol., 47, 12912-
695 12919, doi:10.1021/es401727e, 2013.

696 Guo, S., Hu, M., Wang, Z. B., Slanina, J., and Zhao, Y. L.: Size-resolved aerosol water-
697 soluble ionic compositions in the summer of Beijing: implication of regional
698 secondary formation, Atmos. Chem. Phys., 10, 947-959, doi:10.5194/acp-10-
699 947-2010, 2010.

700 He, H., Li, C., Loughner, C. P., Li, Z., Krotkov, N. A., Yang, K., Wang, L., Zheng, Y., Bao,
701 X., Zhao, G., and Dickerson, R. R.: $SO_2$ over central China: Measurements,
702 numerical simulations and the tropospheric sulfur budget, J. Geophys. Res.-
703 Atmos., 117, D00K37, doi:10.1029/2011JD016473, 2012.

704 Henry, R. C., Chang, Y.-S., and Spiegelman, C. H.: Locating nearby sources of air
705 pollution by nonparametric regression of atmospheric concentrations on wind
706 direction, Atmos. Environ., 36, 2237-2244, 2002.

707 Jayamurugan, R., Kumaravel, B., Palanivelraja, S., and Chockalingam, M. P.: Influence
708 of Temperature, Relative Humidity and Seasonal Variability on Ambient Air
709 Quality in a Coastal Urban Area, International Journal of Atmospheric Sciences,
710 2013, 1-7, doi:10.1155/2013/264046, 2013.

711 Lee, C., Martin, R. V., van Donkelaar, A., Lee, H., Dickerson, R. R., Hains, J. C., Krotkov,
712 N., Richter, A., Vinnikov, K., and Schwab, J. J.: $SO_2$ emissions and lifetimes:
713 Estimates from inverse modeling using in situ and global, space-based
714 (SCIAMACHY and OMI) observations, J. Geophys. Res., 116, doi:10.1029/2010
715 jd014758, 2011.

716 Lin, W., Xu, X., Zhang, X., and Tang, J.: Contributions of pollutants from North China
717 Plain to surface ozone at the Shangdianzi GAW Station, Atmos. Chem. Phys., 8,
718 5889-5898, doi:10.5194/acp-8-5889-2008, 2008.

719 Lin, W., Xu, X., Ge, B., and Zhang, X.: Characteristics of gaseous pollutants at
720 Gucheng, a rural site southwest of Beijing, J. Geophys. Res., 114, D00G14,
721 doi:10. 1029/2008JD010339, 2009.

722 Lin, W., Xu, X., Ge, B., and Liu, X.: Gaseous pollutants in Beijing urban area during the
723 heating period 2007–2008: variability, sources, meteorological, and chemical
724 impacts, Atmos. Chem. Phys., 11, 8157-8170, doi:10.5194/acp-11-8157-2011,
725 2011.

726 Matsui, H., Koike, M., Kondo, Y., Takegawa, N., Kita, K., Miyazaki, Y., Hu, M., Chang, S.
727 Y., Blake, D. R., Fast, J. D., Zaveri, R. A., Streets, D. G., Zhang, Q., and Zhu, T.:
728 Spatial and temporal variations of aerosols around Beijing in summer 2006:
729 Model evaluation and source apportionment, J. Geophys. Res.-Atmos.,114,
730 D00G13, doi:10.1029/2008JD010906, 2009.

731 Parrish, D. D., and Zhu, T.: Clean Air for Megacities, Science, 326, 674-675,
732 doi:10.1126/science.1176064, 2009.

733 Qin, M., Xie, P. H., Wu, D. X., Xu, J., Si, F. Q., Wang, M. H., Dou, K., Zhang, Y., Xiao, X.,
734 Liu, W. S., Liu, S. S., Wang, F. P., Fang, W., Liu, J. G., and Liu, W. Q.: Investigation
735 of variation characteristics and levels of $SO_2$-$NO_2$-$O_3$ and pm10 in Beijing during
736 2008 Olympic Games, J. Atmos. Environ. Opt., 4, 329– 340, 2009.

737 Shao, M., Tang, X., Zhang, Y., and Li, W.: City Clusters in China: Air and Surface Water
738 Pollution, Front. Ecol. Environ., 4, 353-361, 2006.

739 Sander, S. P., J. Abbatt, J. R. Barker, J. B. Burkholder, R. R. Friedl, D. M. Golden, R. E.
740 Huie, C. E. Kolb, M. J. Kurylo, G. K. Moortgat, V. L. Orkin and P. H. Wine
741 "Chemical Kinetics and Photochemical Data for Use in Atmospheric Studies,
742 Evaluation No. 17," JPL Publication 10-6, Jet Propulsion Laboratory, Pasadena,
743 http://jpldataeval.jpl.nasa.gov, 2011.

744 Streets, D. G., Fu, J. S., Jang, C. J., Hao, J., He, K., Tang, X., Zhang, Y., Wang, Z., Li, Z.,
745 Zhang, Q., Wang, L., Wang, B., and Yu, C.: Air quality during the 2008 Beijing
746 Olympic Games, Atmos. Environ., 41, 480-492,2007.

747 Takegawa, N., Miyakawa, T., Kuwata, M., Kondo, Y., Zhao, Y., Han, S., Kita, K., Miyazaki,
748 Y., Deng, Z., Xiao, R., Hu, M., van Pinxteren, D., Herrmann, H., Hofzumahaus, A.,
749 Holland, F., Wahner, A., Blake, D. R., Sugimoto, N., and Zhu, T.: Variability of
750 submicron aerosol observed at a rural site in Beijing in the summer of 2006, J.
751 Geophys. Res., 114, D00G05, doi:10.1029/2008jd010857, 2009.

752 Tang, X. Y.: The characteristics of urban air pollution in China, in Urbanization, Energy,
753 and Air Pollution in China, pp. 47–54, Natl. Acad. Press, Washington, D. C.,2004.

754 Wang, M., Zhu, T., Zheng, J., Zhang, R. Y., Zhang, S. Q., Xie, X. X., Han, Y. Q., and Li, Y.:
755 Use of a mobile laboratory to evaluate changes in on-road air pollutants during
756 the Beijing 2008 Summer Olympics, Atmos. Chem. Phys., 9, 8247-8263,
757 doi:10.5194/acp-9-8247-2009, 2009.

758 Wang, M., Zhu, T., Zhang, J. P., Zhang, Q. H., Lin, W. W., Li, Y., and Wang, Z. F.: Using a
759 mobile laboratory to characterize the distribution and transport of sulfur dioxide
760 in and around Beijing, Atmos. Chem. Phys., 11, 11631-11645, doi:10.5194/acp-
761 11-11631-2011, 2011.

762 Wang, S., Li, G. G., Gong, Z. Y., Du, L., Zhou, Q. T., Meng, X. Y., Xie, S. Y., Zhou. L.,
763 Spatial distribution, seasonal variation and regionalization of $PM_{2.5}$
764 concentrations in China. SCIENCE CHINA Chemistry, 58 (9): 1435-1443, 2015.

765 Wang, T., Ding, A., Gao, J., and Wu, W. S.: Strong ozone production in urban plumes
766 from Beijing, China, Geophys. Res. Lett., 33, L21806, doi:10.1029/2006GL02
767 7689, 2006.

768 Wang, T., Nie, W., Gao, J., Xue, L. K., Gao, X. M., Wang, X. F., Qiu, J., Poon, C. N.,
769 Meinardi, S., Blake, D., Wang, S. L., Ding, A. J., Chai, F. H., Zhang, Q. Z., and
770 Wang, W. X.: Air quality during the 2008 Beijing Olympics: secondary pollutants
771 and regional impact, Atmos. Chem. Phys., 10, 7603–7615, doi:10.5194/acp-10-
772 7603-2010, 2010.

773 Wang, Y. Q., Zhang, X. Y., and Draxler, R. R.: TrajStat: GIS-based software that uses
774 various trajectory statistical analysis methods to identify potential sources from

775 long-term air pollution measurement data, Environmental Modelling &
776 Software, 24, 938-939, 10.1016/j.envsoft.2009.01.004, 2009.

777 Wehner, B., Birmili, W., Ditas, F., Wu, Z., Hu, M., Liu, X., Mao, J., Sugimoto, N., and
778 Wiedensohler, A.: Relationships between submicrometer particulate air
779 pollution and air mass history in Beijing, China, 2004–2006, Atmos. Chem. Phys.,
780 8, 6155-6168, doi:10.5194/acp-8-6155-2008, 2008.

781 Westmoreland, E. J., Carslaw, N., Carslaw, D. C., Gillah, A., and Bates, E.: Analysis of
782 air quality within a street canyon using statistical and dispersion modelling
783 techniques, Atmos. Environ., 41, 9195-9205, 2007.

784 White, W. H., Anderson, J. A., Blumenthal, D. L., Husar, R. B., Gillani, N. V., Husar, J. D.,
785 and Wilson, W. E.: Formation and transport of secondary air pollutants: ozone
786 and aerosols in the St. Louis urban plume, Science, 194, 187–189, 1976.

787 Wu, Q. Z., Wang, Z. F., Gbaguidi, A., Gao, C., Li, L. N., and Wang, W.: A numerical
788 study of contributions to air pollution in Beijing during CAREBeijing-2006,
789 Atmos. Chem. Phys., 11, 5997-6011, doi:10.5194/acp-11-5997-2011, 2011.

790 Xu, J., Ma, J. Z., Zhang, X. L., Xu, X. B., Xu, X. F., Lin, W. L., Wang, Y., Meng, W., and Ma,
791 Z. Q.: Measurements of ozone and its precursors in Beijing during summertime:
792 impact of urban plumes on ozone pollution in downwind rural areas, Atmos.
793 Chem. Phys., 11, 12241-12252, doi:10.5194/acp-11-12241-2011, 2011.

794 Xu, X., Zhou, L., Zhou, X., Yan, P., Weng, Y., Tao, S., Mao, J., Ding, G., Bian, L., and Jhon,
795 C.: Influencing domain of peripheral sources in the urban heavy pollution
796 process of Beijing, Science in China, 48, 565-575, 2005.

797 Yuan, Z., Lau, A. K. H., Shao, M., Louie, P. K. K., Liu, S. C., and Zhu, T.: Source analysis
798 of volatile organic compounds by positive matrix factorization in urban and rural
799 environments in Beijing, J. Geophys. Res., 114, D00G15, doi:10.1029/2008
800 jd011190, 2009.

801 Zhang, J. P., Zhu, T., Zhang, Q. H., Li, C. C., Shu, H. L., Ying, Y., Dai, Z. P., Wang, X., Liu,
802 X. Y., Liang, A. M., Shen, H. X., and Yi, B. Q.: The impact of circulation patterns on

regional transport pathways and air quality over Beijing and its surroundings, Atmos. Chem. Phys., 12, 5031-5053, doi:10.5194/acp-12-5031-2012, 2012.

Zhang, Q., Yuan, B., Shao, M., Wang, X., Lu, S., Lu, K., Wang, M., Chen, L., Chang, C. C., and Liu, S. C.: Variations of ground-level $O_3$ and its precursors in Beijing in summertime between 2005 and 2011, Atmos. Chem. Phys., 14, 6089-6101, doi:10.5194/acp-14-6089-2014, 2014.

Zhang, R., Jing, J., Tao, J., Hsu, S. C., Wang, G., Cao, J., Lee, C. S. L., Zhu, L., Chen, Z., Zhao, Y., and Shen, Z.: Chemical characterization and source apportionment of $PM_{2.5}$ in Beijing: seasonal perspective, Atmos. Chem. Phys., 13, 7053-7074, doi: 10.5194/acp-13-7053-2013, 2013.

Zhou, Y., Wu, Y., Yang, L., Fu, L., He, K., Wang, S., Hao, J., Chen,J., and Li, C.: The impact of transportation control measures on emission reductions during the 2008 Olympic Games in Beijing, China, Atmos. Environ., 44, 285–293, 2010.

Zhu, L., Huang, X., Shi, H., Cai, X., and Song, Y.: Transport pathways and potential sources of $PM_{10}$ in Beijing, Atmos. Environ., 45, 594-604, 2011.

Zhu, Y., Zhang, J., Wang, J., Chen, W., Han, Y., Ye, C., Li, Y., Liu, J., Zeng, L., Wu, Y., Wang, X., Wang, W., Chen, J., and Zhu, T.: Distribution and Sources of Air pollutants in the North China Plain Based on On-Road Mobile Measurements, Atmos. Chem. Phys. Discuss., doi:10.5194/acp-2016-410, in review, 2016.

828 **Table 1.** The overview of measurement instruments.

| Species/ Parameter | Instrument | Detection limit | Time resolution | Precision | Uncertainty |
|---|---|---|---|---|---|
| $SO_2$ | Ecotech 9850B | 0.3 ppb | 1 min | 0.5% (1ppb) | 5% |
| NO-$NO_x$ | Ecotech 9841B | 50 ppb | 1 min | 1% (0.5ppb) | 10% |
| CO | Ecotech 9830 | 0.4 ppb | 1 min | 1% (0.1ppm) | 1% |
| $O_3$ | Ecotech 9810B | 0.5 ppb | 1 min | 0.5% (1ppb) | 5% |
| WS | LASTEM | - | 10 min | 0,1 m $s^{-1}$ | 5% |
| WD | LASTEM | - | 10 min | 0,1 º | 1% |
| BP | LASTEM | - | 10 min | 0,1 hPa | ±0.35 hPa |
| T | LASTEM | - | 10 min | 0,1 ℃ | ±0.2°C |
| RH | LASTEM | - | 10 min | 1% | ±3% |

829

830 **Table 2.** The total and seasonal net surface flux intensities (mean±SD) (μg $s^{-1}$ $m^{-2}$) of

831 gaseous pollutants at the Yufa site from 1 September 2006 to 31 August 2008.

| Flux (μg $s^{-1}$ $m^{-2}$) | $SO_2$ | NO | $NO_2$ | $NO_x$ | CO | $O_3$ | $O_x$ |
|---|---|---|---|---|---|---|---|
| Autumn_06 | 5.3±79.6 | -6.3±27.5 | -3±60.2 | -9.4±78.9 | -30±2730 | 19.4±128.8 | 25.9±177.6 |
| Autumn_07 | 6.3±78.8 | -6.6±33.6 | -3.5±74.3 | -10.1±98.6 | -60±2570 | 10±120 | 6.6±170.3 |
| Winter_06/07 | 11.8±139.1 | -6.9±47.7 | 3.6±105.6 | -3.3±142.9 | 350±4150 | -11.9±127.5 | -8.3±188 |
| winter_07/08 | -13.1±113.3 | -11.5±46.5 | -11±82.3 | -22.6±117.6 | -550±3380 | -29.6±143.1 | -40.7±191.2 |
| Spring_07 | 11.3±90.5 | -1.9±12.1 | 0.1±71.1 | -1.9±78.8 | 50±2720 | 3.4±261.8 | 3.5±315.5 |
| Spring_08 | 13.5±92 | -1.8±15.2 | 0.2±76.4 | -1.5±87 | 160±2630 | 10.7±266.4 | 10.9±321.2 |
| Summer_07 | 11±35.3 | 0.4±6.7 | 8.4±46.9 | 8.7±51.5 | 600±1960 | 71.3±175.7 | 79.7±211.4 |
| Summer_08 | 5.7±26.1 | 0.1±4.9 | 1±32.7 | 1.1±36.6 | 120±1540 | 48.1±183.3 | 49.1±207.8 |
| Total | 6.2±89.5 | -4.3±29.5 | -0.6±72.3 | -4.9±93 | 70±2830 | 14.7±187.8 | 14.8±234.9 |

832

833 **Table 3.** The total and seasonal In surface flux intensities (mean±SD) (i.e. Flux_In,

834 from NCP to Yufa, μg $s^{-1}$ $m^{-2}$) of gaseous pollutants at the Yufa site from 1 September

835 2006 to 31 August 2008.

| Flux_In (μg $s^{-1}$ $m^{-2}$) | $SO_2$ | NO | $NO_2$ | $NO_x$ | CO | $O_3$ | $O_x$ |
|---|---|---|---|---|---|---|---|
| Autumn_06 | 53.3±62.7 | 5.1±7.9 | 42.5±34.3 | 47.6±37.9 | 1770±1740 | 85±131.6 | 143.1±158.3 |
| Autumn_07 | 43.9±80.8 | 8.5±14.5 | 48.7±51.8 | 57.2±60.7 | 1720±1820 | 65.1±116.8 | 117.3±140.2 |
| Winter_06/07 | 106.3±126.1 | 19.8±30 | 82.3±83 | 102±101.5 | 3360±3620 | 40.1±74.1 | 122.4±112.8 |
| winter_07/08 | 72.3±95.1 | 13.6±20.9 | 60.4±60.2 | 74±72.6 | 2170±2130 | 41.7±70.2 | 102.1±98.3 |
| Spring_07 | 62.9±88.3 | 3.8±7.2 | 53.6±46.6 | 57.5±49.7 | 1970±2050 | 158.8±193.2 | 212.5±223.1 |
| Spring_08 | 64.7±97.5 | 6±9 | 56.8±44.6 | 62.7±49.1 | 2090±1850 | 162.5±194.4 | 222.9±217.9 |
| Summer_07 | 22.3±38.7 | 2.9±5.4 | 32.4±30.1 | 35.3±32.4 | 1560±1630 | 140.7±177.9 | 173.1±199.7 |
| Summer_08 | 18.9±24.3 | 2.8±2.6 | 20.8±16.3 | 23.6±18.2 | 1060±880 | 138.2±168.9 | 160.1±180.2 |
| Total | 53.2±84.8 | 7.4±15.4 | 48.3±51.5 | 55.8±60.7 | 1920±2130 | 108.2±159.2 | 159.7±180 |

836 **Table 3.** (Continuous) The total and seasonal Out surface transport flux intensities

837 (mean±SD) (i.e. Flux_Out, from Beijing to Yufa, μg $s^{-1}$ $m^{-2}$) of gaseous pollutants at the

838 Yufa site from 1 September 2006 to 31 August 2008.

| Flux_Out ($\mu g\ s^{-1}\ m^{-2}$) | $SO_2$ | NO | $NO_2$ | $NO_x$ | CO | $O_3$ | $O_x$ |
|---|---|---|---|---|---|---|---|
| Autumn_06 | -40.4±66 | -17.8±34.4 | -48.6±43.9 | -66.4±67.3 | -1830±2360 | -44.7±87.5 | -91.2±103.4 |
| Autumn_07 | -30.2±56.5 | -21.4±39.9 | -54.5±54.9 | -75.9±82.9 | -1800±1910 | -48.9±92.3 | -101.5±120.4 |
| Winter_06/07 | -72.8±86 | -30.7±48.1 | -66.8±67.6 | -97.6±103.8 | -2350±2380 | -58.4±146.3 | -125.2±163.9 |
| winter_07/08 | -73.9±81.6 | -29.5±51.2 | -61.9±52.9 | -91.3±92.4 | -2490±2690 | -80.4±159.2 | -142.3±175.7 |
| Spring_07 | -41.3±55.8 | -7.8±13.2 | -54.6±45.6 | -62.4±52.6 | -1920±1720 | -155.2±225 | -209.8±245.6 |
| Spring_08 | -38.8±44.4 | -9.7±16.2 | -57.4±56.4 | -67.1±65.8 | -1820±1660 | -151.3±235.8 | -205.2±259.7 |
| Summer_07 | -9±13.3 | -4.2±6.5 | -34.2±40.8 | -38.4±44.9 | -1110±1210 | -51.6±76.6 | -85.8±102.2 |
| Summer_08 | -12.1±15.8 | -3.5±5 | -25.6±30.1 | -29.1±33.3 | -1150±1320 | -75.2±119.5 | -100.1±137.1 |
| Total | -42.8±64.6 | -16.7±35.2 | -52±52.8 | -68.7±77.1 | -1870±2080 | -85±163.2 | -137.3±184.5 |

**Table 4.** The mean surface transport flux (i.e. Flux_2007), the influx (i.e. the positive surface flux, from the NCP to Yufa, In_2007 and In_2008), the outflux (i.e. the negative surface flux, from Beijing to Yufa, Out_2007 and Out_2008), and the mean concentration during the 2008 Beijing Olympic period (from 8 August 2008 to 20 September 2008) and the same corresponding period of 2007 (from 8 August 2007 to 20 September 2007).

| Flux ($\mu g\ s^{-1}\ m^{-2}$) | Flux_2007 | In_2007 | Out_2007 | Flux_2008 | In_2008 | Out_2008 | Cont._2007 (ppb) | Cont._2008 (ppb) |
|---|---|---|---|---|---|---|---|---|
| $SO_2$ | 7.9±19.3 | 14.9±20.8 | -4.5±4.6 | 1.4±15.5 | 11.9±13.6 | -9±8.8 | 3.6±3.4 | 3.9±2.2 |
| NO | 0.3±8.6 | 3.8±5 | -5.9±9.9 | -0.1±3.2 | 2.4±1.8 | -2.5±2.3 | 4.3±5.5 | 1.9±0.6 |
| $NO_2$ | 4.1±37.9 | 24.1±18.6 | -31.3±37.9 | -1.3±21.9 | 15.2±11.6 | -17.5±17.1 | 16.1±10.2 | 8.5±3.6 |
| $NO_x$ | 4.4±44.5 | 27.8±20.7 | -37.2±45.3 | -1.4±25 | 17.5±13.2 | -20±19.2 | 20.5±13.3 | 10.4±4 |
| CO | 540±158 | 1390±1160 | -980±980 | 10±1110 | 870±670 | -850±740 | 1190±490 | 750±260 |
| $O_3$ | 60±130 | 117.9±122.6 | -42.6±61.1 | 24.9±124.6 | 110.9±111 | -60.6±63.7 | 41.1±30.5 | 38.9±25.8 |
| $O_x$ | 64.1±154.4 | 141.9±129.1 | -73.9±82.4 | 23.7±142.1 | 126.7±118.4 | -77.7±74.6 | 57.2±27.3 | 47.4±24.1 |

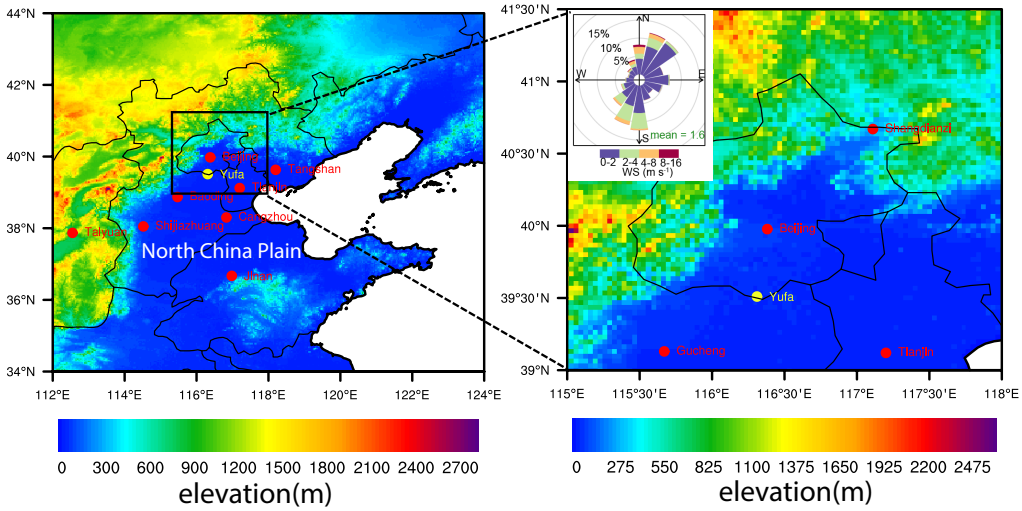


846

847 **Figure 1.** The location information of the Yufa site.

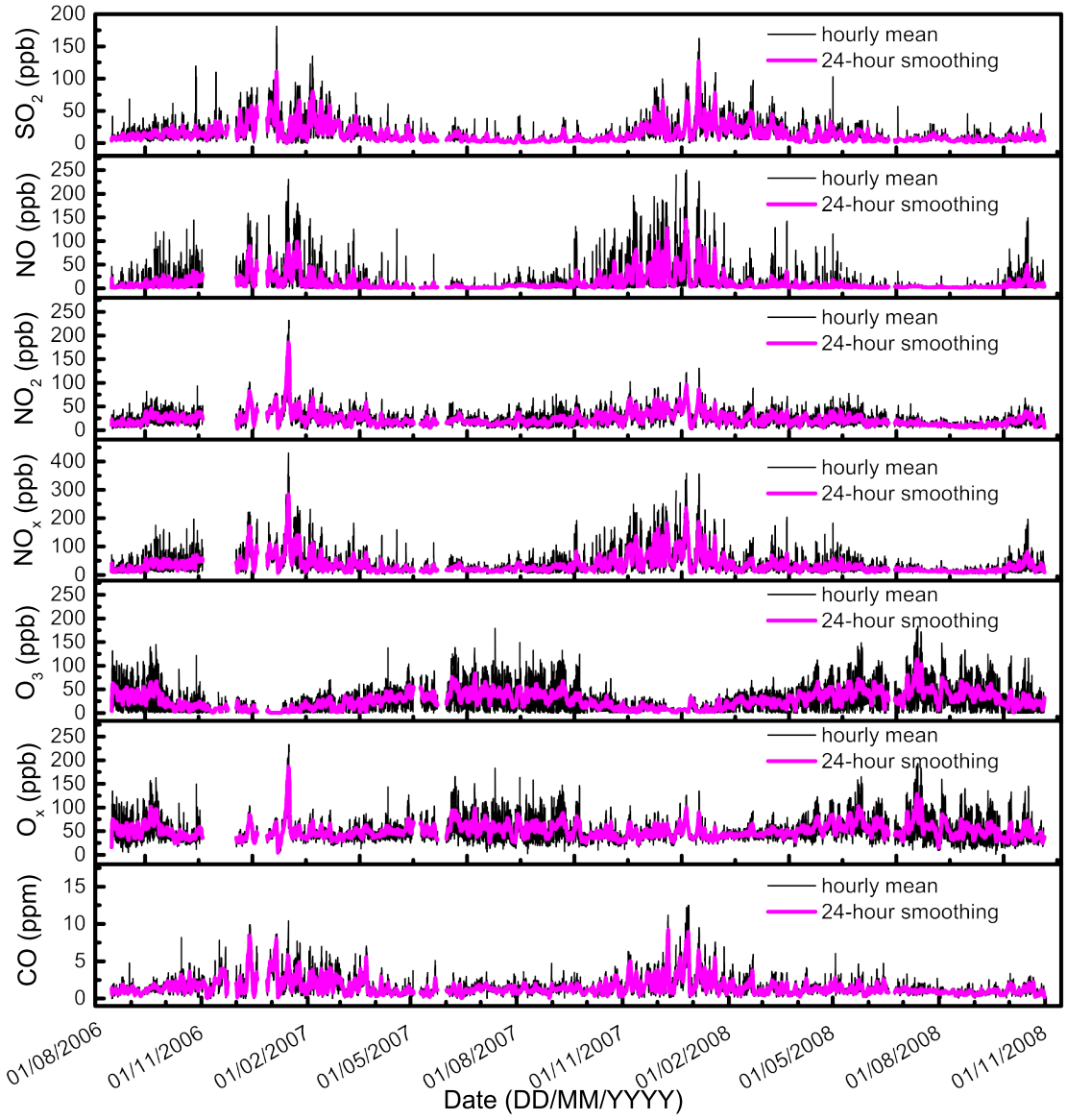


848

849 **Figure 2.** Time series of hourly mean (black line) and 24-hour smoothing (red line)

850 concentrations of $SO_2$, NO, $NO_2$, $NO_x$, $O_3$, $O_x$, and CO at the Yufa site from 15 August

851 2006 to 31 October 2008.

852

853

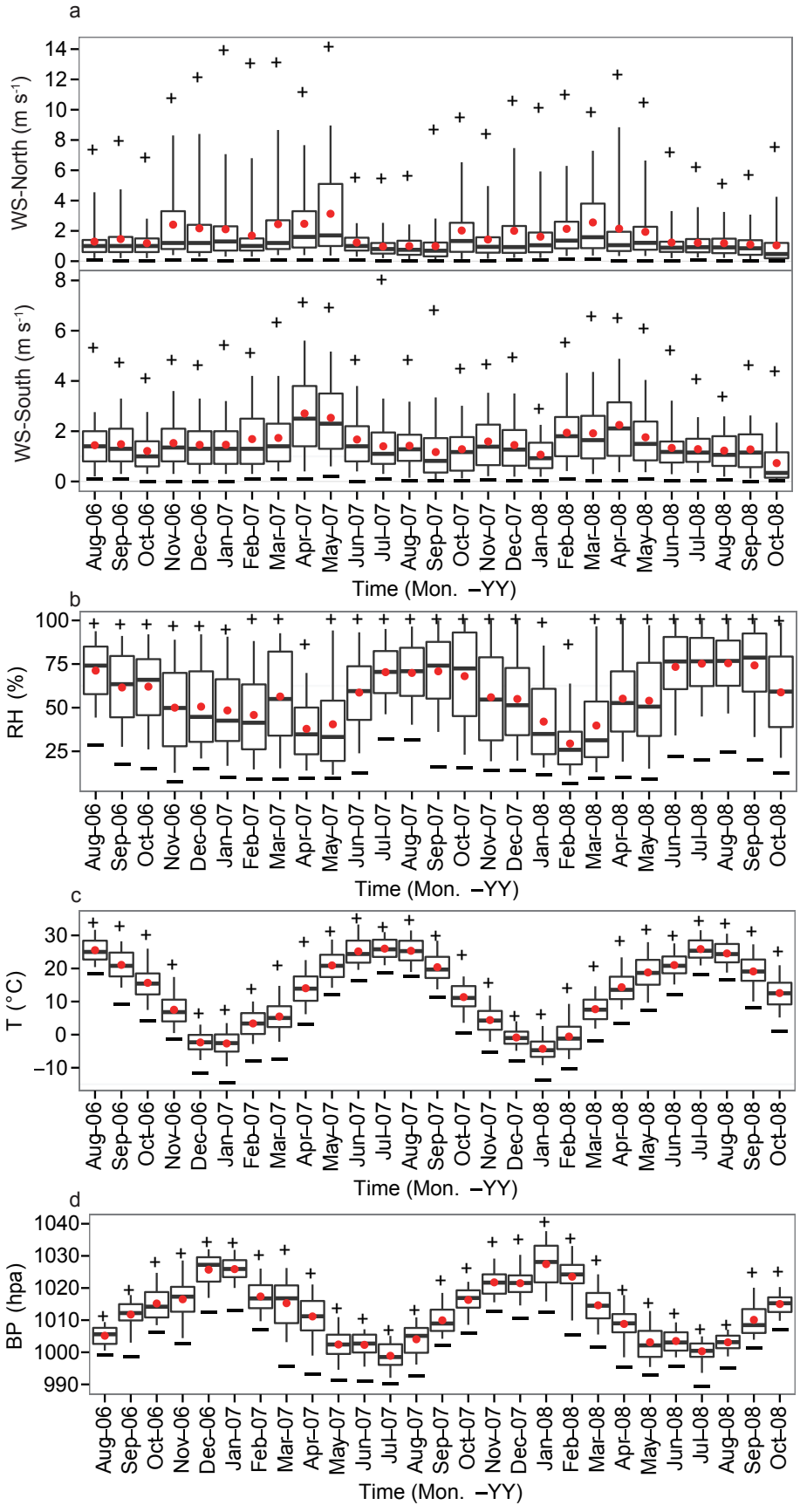
a
WS-North (m s-1)
WS-South (m s-1)
Time (Mon. –YY)
b
RH (%)
Time (Mon. –YY)
c
T (°C)
Time (Mon. –YY)
d
BP (hpa)
Time (Mon. –YY)
Aug–06
Sep–06
Oct–06
Nov–06
Dec–06
Jan–07
Feb–07
Mar–07
Apr–07
May–07
Jun–07
Jul–07
Aug–07
Sep–07
Oct–07
Nov–07
Dec–07
Jan–08
Feb–08
Mar–08
Apr–08
May–08
Jun–08
Jul–08
Aug–08
Sep–08
Oct–08

854

**Figure 3.** Monthly statistics of wind speed (WS) for north wind (a) top and south wind (a) bottom, relative Humidity (RH) (b), temperature (T) (c) and barometric pressure (BP) (d) at the Yufa site. The red point represents the mean value. The black cross bar stands for the median value. The black box and whisker denote the 5th, 25th, 75th and 95th percentiles, respectively. The plus and minus symbols represent the maximum and minimum, respectively. It should be clarified that the North and South wind here is different from the wind direction definition in meteorology. The South wind here is the wind with direction from 90° to 270°, while the North wind is from 0° to 90° and from 270° to 360°.

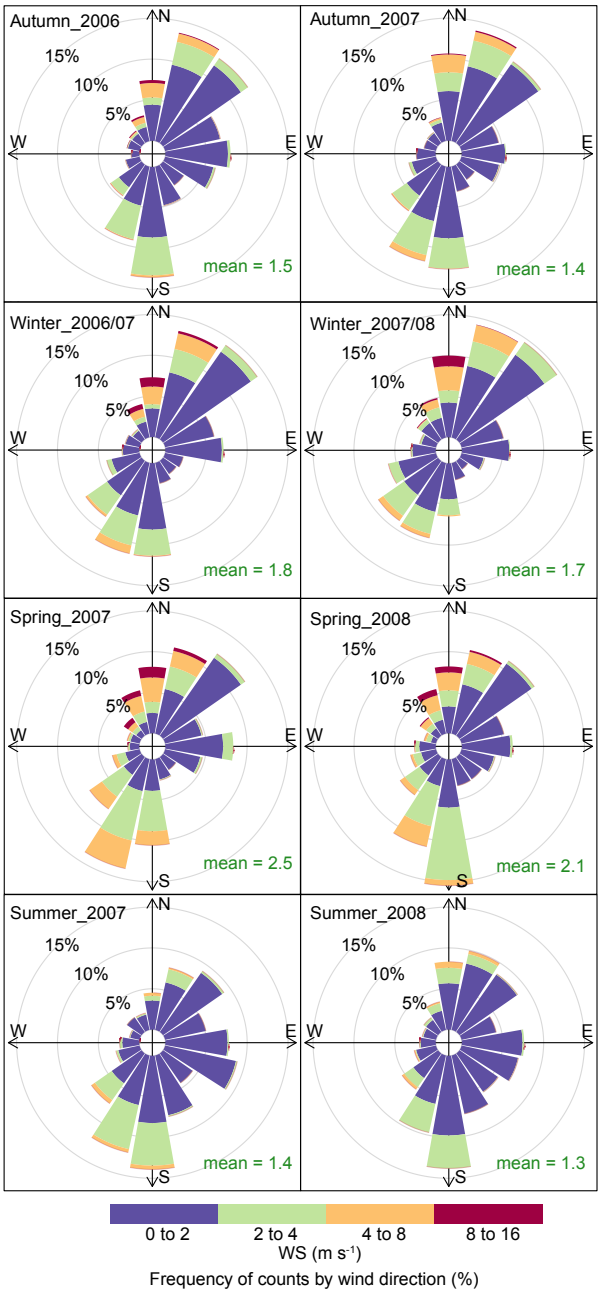


865

866 **Figure 4.** Wind rose plots based on frequencies of hourly data in Autmun_2006,
867 Autumn_2007, Winter_2006/07, Winter_2007/08, Spring_2007, Spring_2008,
868 Summer_2007, Summer_2008. Spring (MAM): March, April, and May; Summer (JJA):
869 June, July, and August; Autumn (SON): September, October, and November; Winter
870 (DJF): December, January, and February.

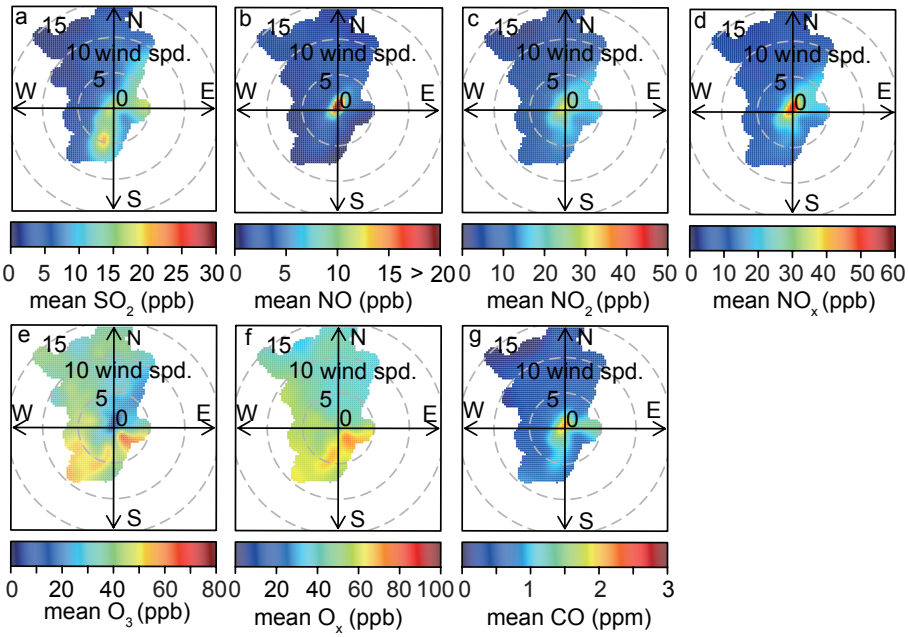


871

872 **Figure 5.** Bivariate polar plots for $SO_2$ (a), NO (b), $NO_2$ (c), $NO_x$ (d), $O_3$ (e), $O_x$ (f) and CO

873 (g) concentrations based on hourly average data at the Yufa site from 1 September

874 2006 to 31 August 2008. The colour scale shows the concentrations of pollutants in

875 ppb (or ppm specially for CO) and the radial scale shows the wind speed (m $s^{-1}$),

876 which increases from the centre of the plot radially outwards.

877

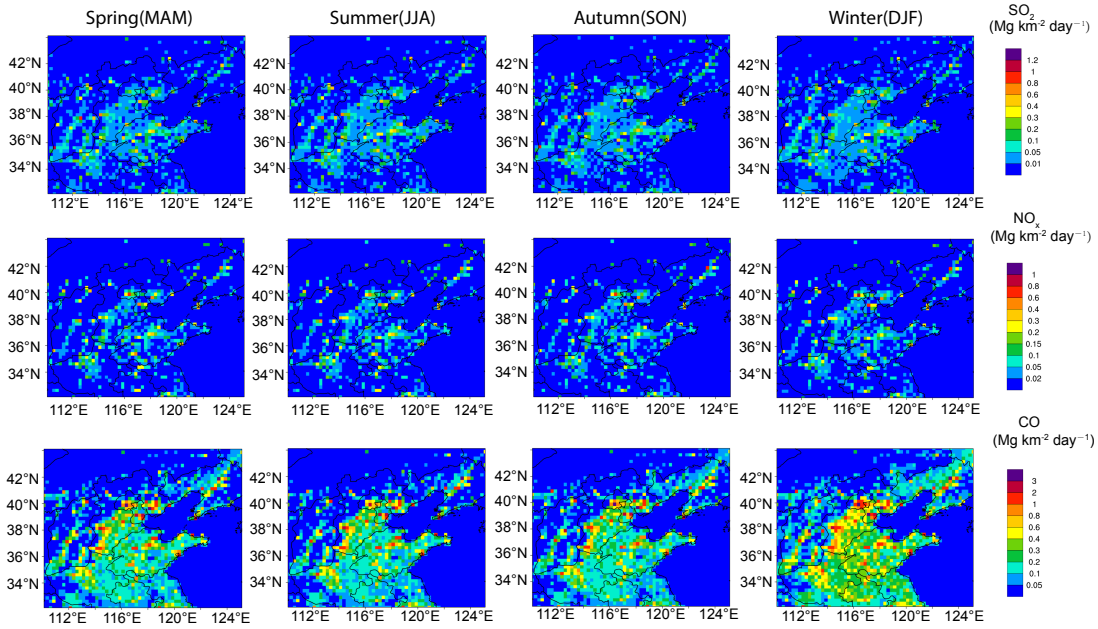


878

879 **Figure 6.** Spatial distribution of seasonal $NO_x$, CO, and $SO_2$ emissions in Northern

880 China in 2008 based on the Multi-resolution Emission Inventory of China (MEIC;

881 www.meicmodel.org) (unit: Mg $km^{-2}$ $day^{-1}$, horizontal resolution: 25 km×25 km).

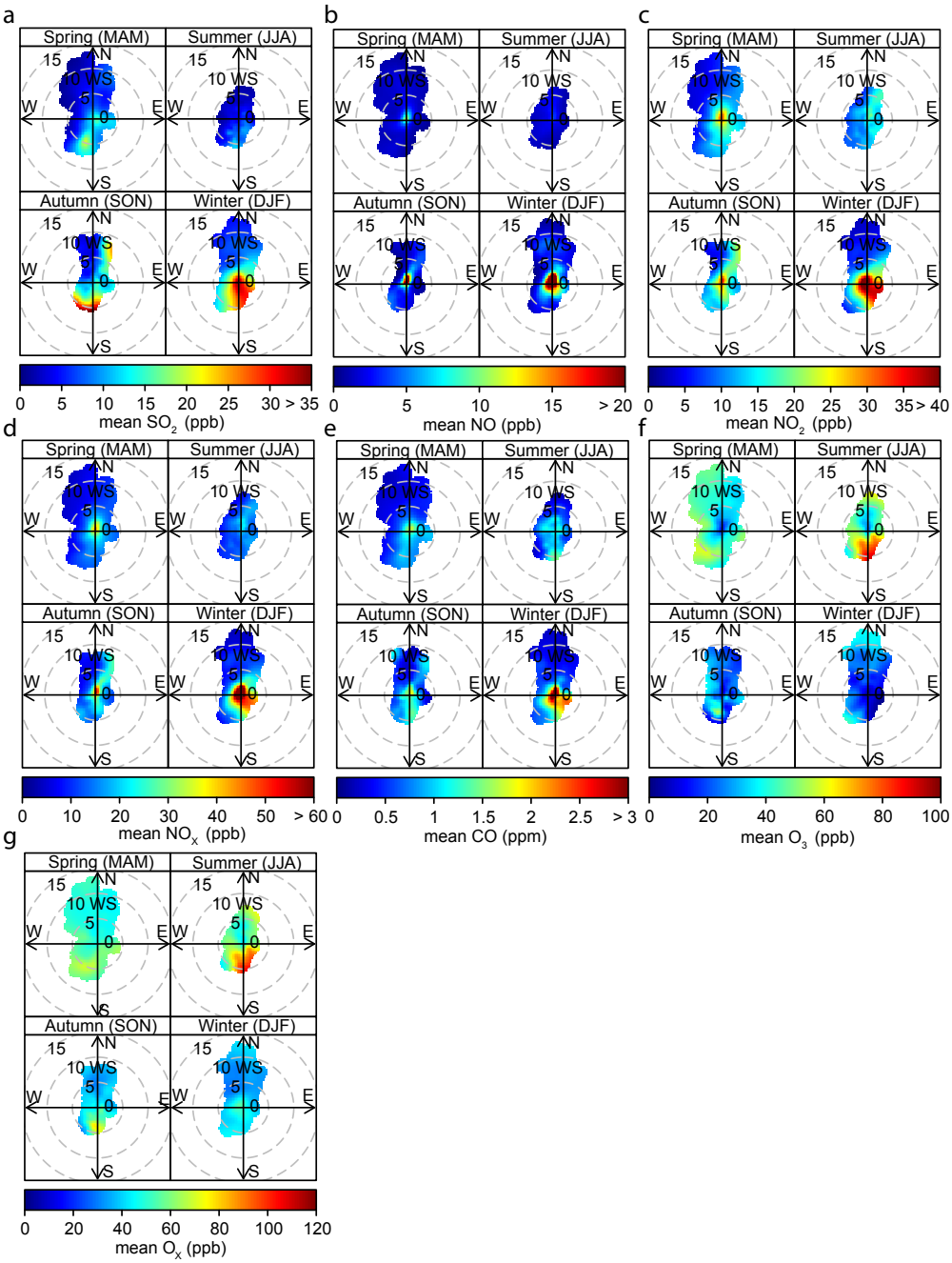


882

883 **Figure 7.** Seasonal bivariate polar plots for $SO_2$ (a), NO (b), $NO_2$ (c), $NO_x$ (d), CO (e), $O_3$

884 (f), $O_x$ (g) and concentrations based on hourly mean data at the Yufa site from 1

885 September 2006 to 31 August 2008. The colour scale shows the concentrations of

886 pollutants in ppb (or ppm specially for CO) and the radial scale shows the wind speed

887 (m $s^{-1}$), which increases from the centre of the plot radially outwards.

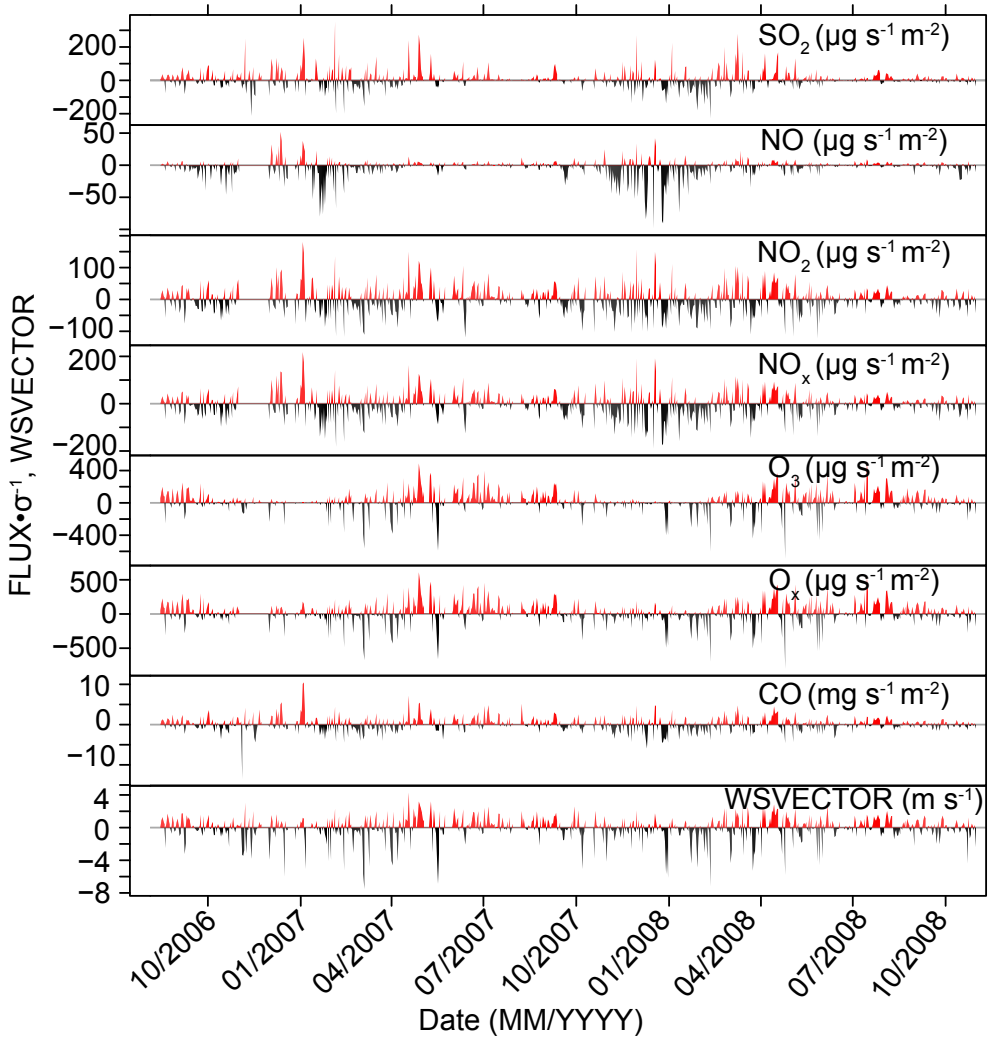


888

889 **Figure 8.** Time series of surface flux intensity (i.e. flux per unit cell, μg $s^{-1}$ $m^{-2}$ or mg

890 $s^{-1}$ $m^{-2}$) for $SO_2$, NO, $NO_2$, $NO_x$, $O_3$, $O_x$, CO and wind vector , i.e. $-\frac{1}{n}\sum_{j=1}^{n} WS_j \cdot cos\theta_j$

891 (WSVECTOR, m $s^{-1}$) based on daily average data at the Yufa site from 15 August 2006

892 to 31 October 2008. The red shaded line indicates the positively transport direction

893 of gaseous pollutants from south to north (i.e. from the NCP to Yufa) and the black

894 shaded line represents the negatively transport direction of gaseous pollutants from

895 north to south (i.e. from Beijing to Yufa).

896

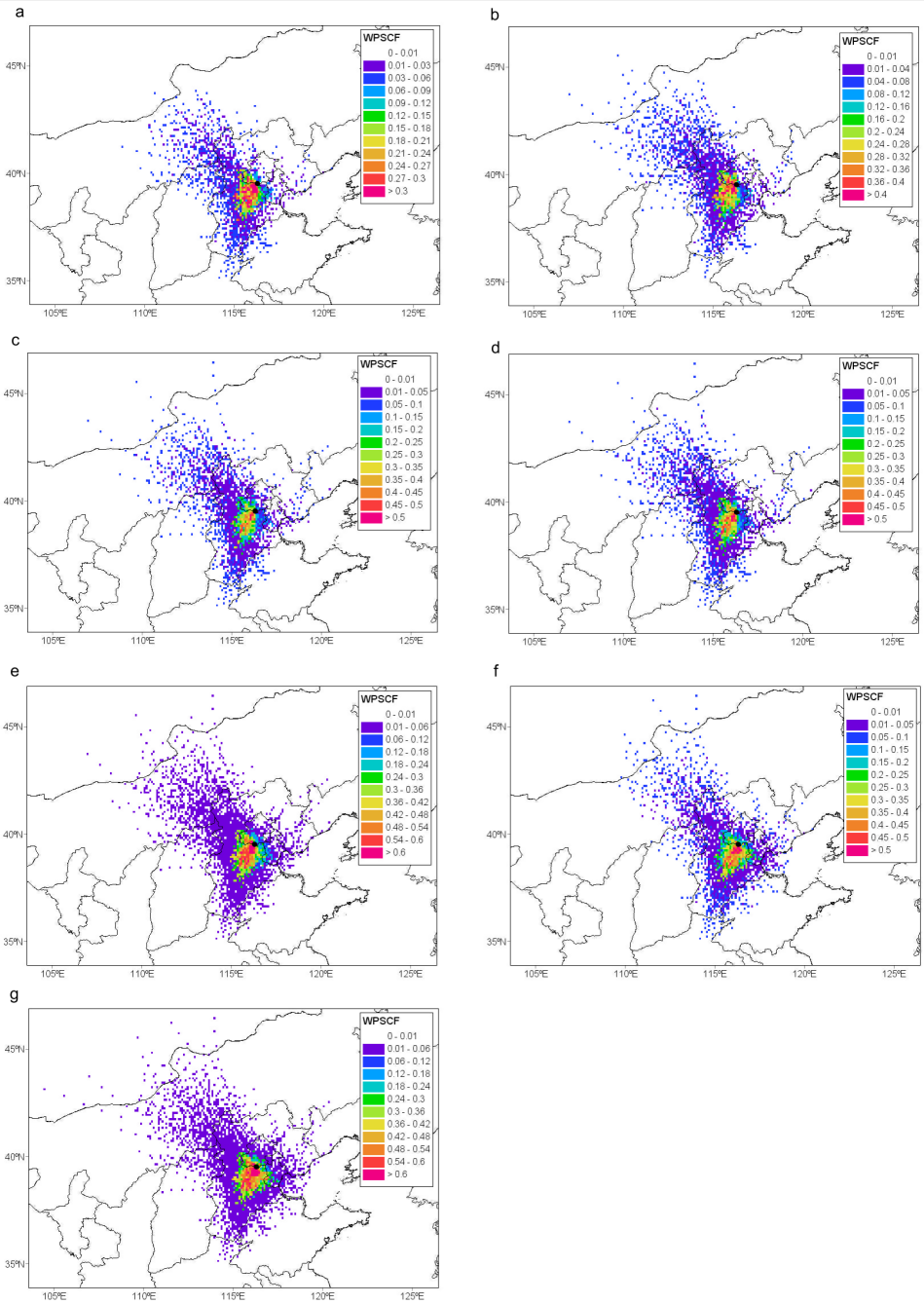


**Figure 9.** The PSCF maps for the $SO_2$ (a), NO (b), $NO_2$ (c), $NO_x$ (d), $O_3$ (e), $O_x$ (f) and CO (g) positive surface flux intensity (i.e from NCP to Yufa). The criterion value of the surface flux intensity is set to greater than 50, 10, 50, 50, 50, 50, and 1000 μg $s^{-1}$ $m^{-2}$ for $SO_2$, NO, $NO_2$, $NO_x$, $O_3$, $O_x$, and CO, respectively.

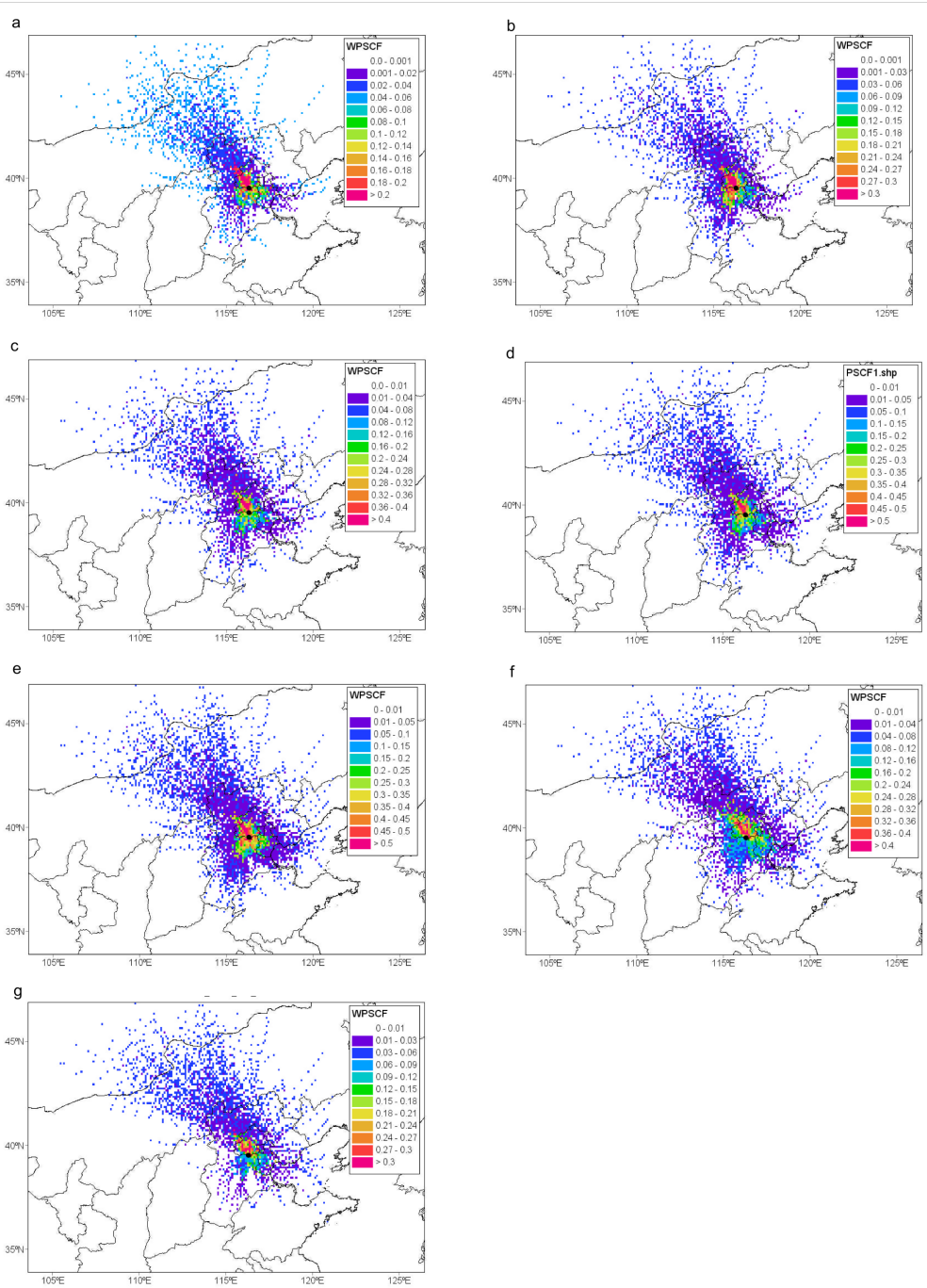


902

903 Figure 10. The PSCF maps for the $SO_2$ (a), NO (b), $NO_2$ (c), $NO_x$ (d), $O_3$ (e), $O_x$ (f) and CO

904 (g) negative surface flux intensity (i.e from Beijing to Yufa). The criterion value of the

905 surface flux intensity is set to lower than -50, -10, -50, -50, -50, -50, and -1000 μg $s^{-1}$

906 $m^{-2}$ for $SO_2$, NO, $NO_2$, $NO_x$, $O_3$, $O_x$, and CO, respectively.

# Observation of regional air pollutant transport between the megacity Beijing and the North China Plain

Yingruo Li[1], Chunxiang Ye[1,2], Jun Liu[1], Yi Zhu[1], Junxia Wang[1], Ziqiang Tan[1], Weili Lin[3], Limin Zeng[1], Tong Zhu[1,4*]

[1]State Key Laboratory of Environmental Simulation and Pollution Control, College of Environmental Sciences and Engineering, Peking University, Beijing, 100871, China

[2]Now at School of Chemistry, University of Leeds, Leeds LS2 9JT, UK

[3]Meteorological Observation Center, China Meteorological Administration, Beijing, 100081, China

[4]The Beijing Innovation Center for Engineering Science and Advanced Technology, Peking University, Beijing, 100871, China

*Corresponding Author: tzhu@pku.edu.cn

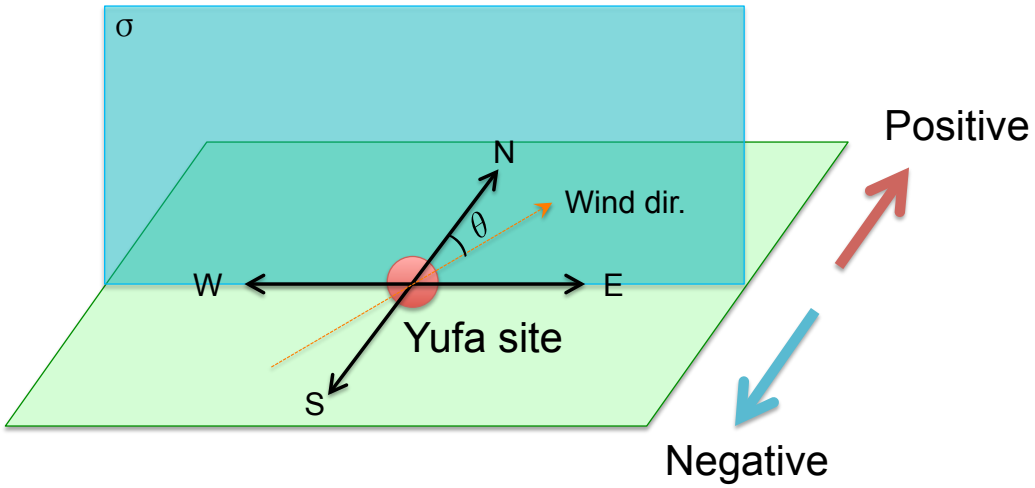


Figure S1. Principles for calculating gaseous pollutant fluxes: the wind vector along the north-south direction multiplies concentration of gaseous pollutant equals the gas pollutant flux. The direction from south to north (i.e. from the NCP to Beijing) is defined as positive, and vice versa.

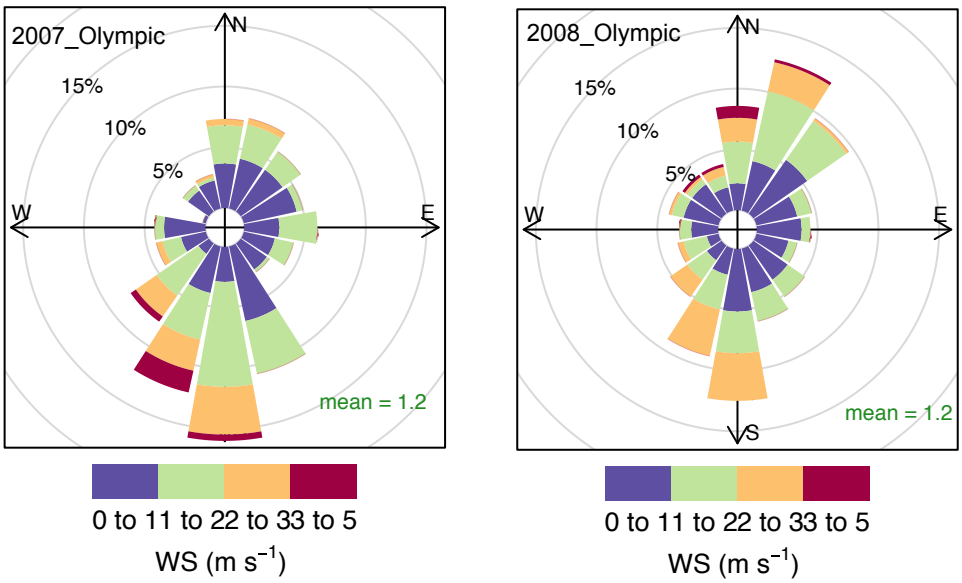


Figure S2. Wind rose plots during the 2008 Beijing Olympic period (from 8 August 2008 to 20 September 2008; 2008_Olympic, Right) and the same corresponding period of 2007 (from 8 August 2007 to 20 September 2007; 2007_Olympic, Left) based on frequencies of hourly data.